iScience

CellPress
OPEN ACCESS

Article

The immune checkpoint ICOSLG is a relapse-predicting biomarker and therapeutic target in infant t(4;11) acute lymphoblastic leukemia

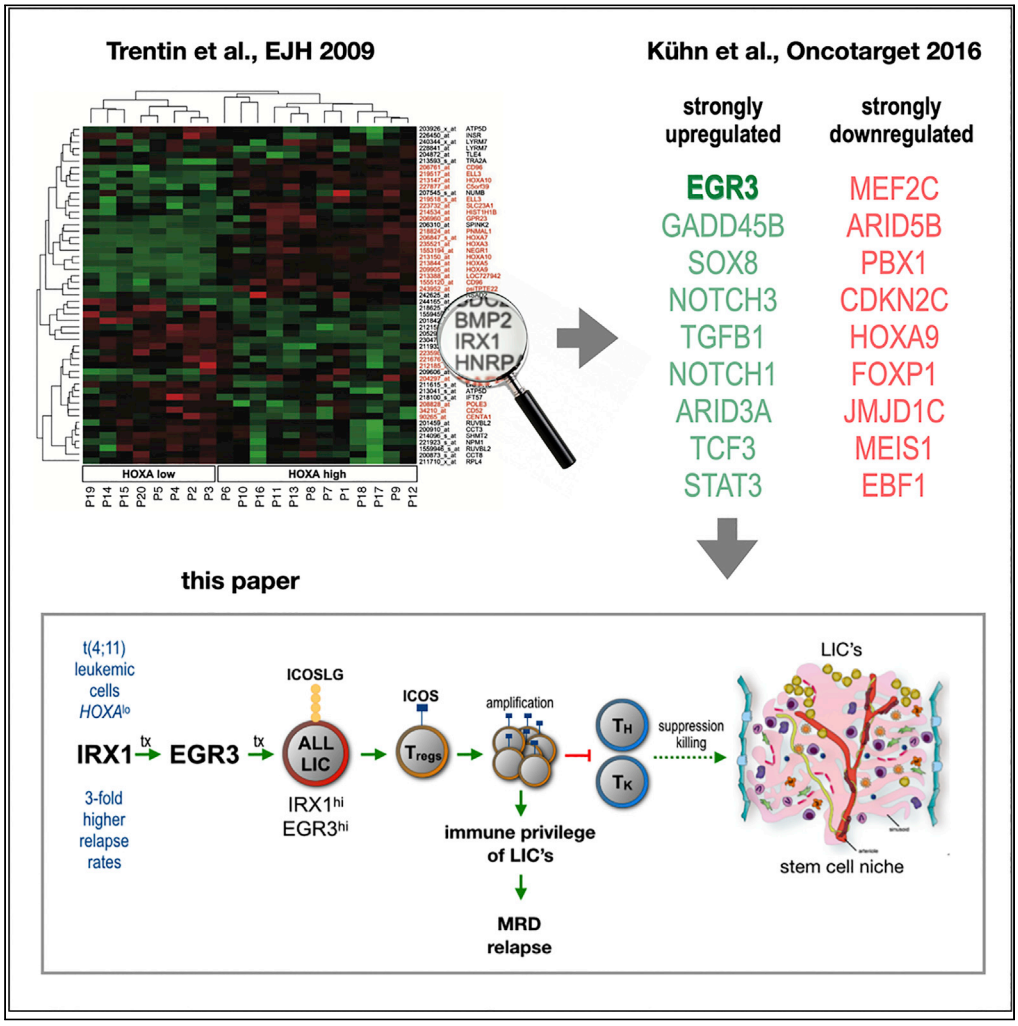

Marius Külp, Anna Lena Siemund, Patrizia Larghero, ..., Halvard Bonig, Claus Meyer, Rolf Marschalek

rolf.marschalek@em.uni-frankfurt.de

Highlights

Early growth response 3 (EGR3) is a direct transactivator of the immune checkpoint gene *ICOSLG*

high *ICOSLG* expression at diagnosis is predictive for ALL relapse

EGR3 and *ICOSLG* expressions are relapse-associated

expression of ICOSLG on t(4;11) ALL cells leads to the rapid expansion of Tregs

Külp et al., iScience *25*, 104613
July 15, 2022
https://doi.org/10.1016/j.isci.2022.104613

iScience

CellPress
OPEN ACCESS

Article

The immune checkpoint ICOSLG is a relapse-predicting biomarker and therapeutic target in infant t(4;11) acute lymphoblastic leukemia

Marius Külp,[1] Anna Lena Siemund,[1] Patrizia Larghero,[1] Alissa Dietz,[1] Julia Alten,[2] Gunnar Cario,[2] Cornelia Eckert,[3] Aurélie Caye-Eude,[4] Hélène Cavé,[4] Michela Bardini,[5] Giovanni Cazzaniga,[5,6] Paola De Lorenzo,[7] Maria Grazia Valsecchi,[8] Laura Diehl,[9,10] Halvard Bonig,[9,10,11] Claus Meyer,[1] and Rolf Marschalek[1,12,*]

SUMMARY

The most frequent genetic aberration leading to infant ALL (iALL) is the chromosomal translocation t(4;11), generating the fusion oncogenes *KMT2A:AFF1* and *AFF1:KMT2A*, respectively. *KMT2A*-r iALL displays a dismal prognosis through high relapse rates and relapse-associated mortality. Relapse occurs frequently despite ongoing chemotherapy and without the accumulation of secondary mutations. A rational explanation for the observed chemo-resistance and satisfactory treatment options remain to be elucidated. We found that elevated *ICOSLG* expression level at diagnosis was associated with inferior event free survival (EFS) in a cohort of 43 patients with t(4;-11) iALL and that a cohort of 18 patients with iALL at relapse displayed strongly increased ICOSLG expression. Furthermore, co-culturing t(4;11) ALL cells (ICOSLG^{hi}) with primary T-cells resulted in the development of T_{regs}. This was impaired through treatment with a neutralizing ICOSLG antibody. These findings imply ICOSLG (1) as a relapse-predicting biomarker, and (2) as a therapeutic target involved in a potential immune evasion relapse-mechanism of infant t(4;11) ALL.

INTRODUCTION

KMT2A-rearrangements (*KMT2A*-r) occur in 70-80% of all infant acute lymphoblastic leukemias (iALL) (Pieters et al., 2007, 2019). Among these, the translocation t(4;11) generating the fusion oncogenes *KMT2A::AFF1* and *AFF1::KMT2A* is the most frequent, accounting for about 49% of all *KMT2A*-r iALL cases (Meyer et al., 2018). *KMT2A*-r is a negative risk factor in iALL with a 4-year event-free survival (4-year-EFS) of only 37% among *KMT2A*-r cases and 36% among t(4;11) cases, respectively. By comparison, patients with *KMT2A*-germline achieve a 4-year-EFS of 74% (Pieters et al., 2007). The typical clinical picture of *KMT2A*-r iALL is that patients initially reach complete remission (CR) during induction therapy but relapse months later despite continuous chemotherapy (Pieters et al., 2007). This results in a 3-year post-relapse overall survival (3-year-OS) of only 17% for patients with t(4;11), with OS defined as the time from relapse to death (Driessen et al., 2016). Designated studies indicate the absence of significant accumulation or selection of secondary mutations in the dominant leukemic clone between the timepoints of diagnosis and relapse (Andersson et al., 2015; Agraz-Doblas et al., 2019). Thus, an explanation for how therapy resistance is achieved remains an open question.

Our group previously identified the C2H2 zinc finger transcription factors *Early growth response 1, 2,* and *3* (EGR1, EGR2, EGR3) as downstream mediators of the transcription factor *Iroquois homeobox 1* (IRX1) (Kühn et al., 2016). Relatively higher transcription of *IRX1* was observed in patients with iALL presenting a low *HOXA* gene expression (Trentin et al., 2009). This *IRX1*^{hi}/*HOXA*^{lo} patient group displayed an increased relapse rate with dismal outcome (Stam et al., 2010; Kang et al., 2012). EGR1, EGR2, EGR3, and their murine homologs have been described to be involved in cell cycle inhibition and stemness of hematopoietic stem cells (HSC) (Min et al., 2008; Cheng et al., 2015; Li et al., 2017). Additionally, EGR3 expression in murine T- and B-cells is known to restrict immune activity and prevent autoimmunity (Safford et al., 2005; Anderson et al., 2006; Collins et al., 2008; Li et al., 2012; Parkinson et al., 2014).

[1]Diagnostic Center of Acute Leukemia (DCAL), Institute of Pharmaceutical Biology, Goethe-University, University of Frankfurt, Max-von-Laue-Str. 9, Frankfurt am Main, Germany

[2]Department of Pediatrics, University Medical Center Schleswig-Holstein, Campus Kiel, Germany

[3]Department of Pediatric Hematology and Oncology, Charité-Universitätsmedizin Berlin, Berlin, Germany

[4]Département de Génétique, Hôpital Robert Debré, Assistance Publique des Hôpitaux de Paris (AP-HP), Paris, France

[5]Centro Ricerca Tettamanti, Pediatrics, University of Milan-Bicocca, Fondazione Monza e Brianza per il Bambino e la sua Mamma (MBBM)/San Gerardo Hospital, Monza, Italy

[6]Genetics, School of Medicine and Surgery, University of Milan-Bicocca, Monza, Italy

[7]Statistical Section, Pediatric Clinic, University of Milano-Bicocca, Monza, Italy

[8]Center of Bioinformatics, Biostatistics and Bioimaging, University of Milano-Bicocca, Monza, Italy

[9]Institute for Transfusion Medicine and Immunohematology, Goethe University, Frankfurt am Main, Germany

[10]German Red Cross Blood Service Baden-Württemberg-Hessen, Frankfurt am Main, Germany

[11]Department of Medicine, Division of Hematology, University of Washington

Continued

We were able to demonstrate that the zinc finger transcription factor *Early growth response 3* (EGR3) binds directly to the promoter of the *ICOSLG* gene and upregulates ICOSLG protein. ICOSLG is an immune checkpoint expressed by antigen-presenting cells (APC) as well as non-lymphoid cells including mesenchymal stem cells, endothelial cells, fibroblasts, and tumor cells (Swallow et al., 1999; Khayyamian et al., 2002; Martin-Orozco et al., 2010; Zhang et al., 2016). ICOSLG belongs to the B7 family of costimulatory immune receptors with partial sequence identity of CD80/CD86 and binds ICOS (Coyle and Gutierrez-Ramos, 2001). ICOS belongs to the CD28 superfamily of immune receptors, is expressed at low levels in resting memory T-cell subsets, but becomes upregulated through ICOSLG binding (Hutloff et al., 1999; Khayyamian et al., 2002). The interaction between ICOSLG and ICOS has been shown to lead to the development of T_{regs} in healthy bone marrow as well as in several tumor microenvironments with clinical implications in melanoma, glioblastoma, breast cancer and acute myeloid leukemia (AML) (Martin-Orozco et al., 2010; Faget et al., 2012; Lee et al., 2017; Han et al., 2018; Iwata et al., 2019).

In summary, we report here that high gene expression of *ICOSLG* at initial diagnosis was associated with inferior EFS in a cohort of 43 infant patients with t(4;11) ALL and that a cohort of 18 patients with infant ALL (iALL) at relapse displayed strongly increased *EGR3* and *ICOSLG* transcription levels. Upregulation of *ICOSLG* expression in t(4;11) ALL cells caused increased development of regulatory T-cells (T_{regs}) when co-cultured with primary T-cells. The development of T_{regs} was impaired through the treatment with a neutralizing α-ICOSLG antibody.

Thereby, we provide a potential relapse mechanism that could explain how *KMT2A*-r leukemia cells reach therapy resistance. Consequently, our study not only suggests *ICOSLG* as a relapse-predicting prognostic biomarker, but identifies the ICOSLG/ICOS interaction as a putative therapeutic target in infant t(4;11) ALL.

RESULTS

Early growth response 3 upregulates *ICOSLG* through direct promoter binding in an early growth response 3-overexpressing t(4;11) SEM cell model

The initial observation that *IRX1* is upregulated in patients with t(4;11) iALL that display a *HOXA*^{lo} signature prompted us to investigate the role of IRX1 in further detail. Overexpression of IRX1 resulted in the transcriptional upregulation of *HOXB4* and the *Early growth response genes EGR1-3* (Kühn et al., 2016). We cloned the *EGR3* open reading frame (ORF) fused to a C-terminal FLAG tag into our sleeping beauty vector system (Kowarz et al., 2015). This vector construct was stably integrated into the genome of the t(4;11) cell line SEM (SEM::EGR3), and transgene expression was induced by the addition of Doxycycline. An empty vector was used for the generation of a stable control cell line (SEM::mock). This cell culture model system enabled us to investigate the effects of *EGR3* overexpression in a t(4;11) pro-B cellular context. Quantitative real-time PCR (qPCR) confirmed transgene expression and revealed strong upregulation of *ICOSLG* by EGR3 ($\Delta\Delta C_T = 3.24 \pm 0.16$) at the transcription level (Figure 1A). We used Western blot experiments to confirm the EGR3 protein expression and the ICOSLG upregulation on the protein level (Figure 1B).

Considering that EGR3 is a zinc finger transcription factor we aimed to investigate whether EGR3 binds directly to the *ICOSLG* promoter or acts as an indirect *ICOSLG* activator. For that purpose, we performed chromatin immunoprecipitation (ChIP) followed by qRT-PCR and ChIP-Seq. ChIP-qRT-PCR and percent input calculation of the SEM::EGR3 cell model demonstrated that EGR3 binds directly to the promoter of the *ICOSLG* gene (Figure 1C). This initial result was later corroborated by ChIP-Seq (Figure 1D).

Iroquois homeobox 1, early growth response 3, and ICOSLG expressions correlate strongly in a cohort of 50 infant patients with t(4;11) pro-B ALL

In order to validate the findings of our experimental model system, we examined the gene expression of 50 infant patients with t(4;11) pro-B ALL using qRT-PCR. Patient characteristics are summarized in Table 1. The age distribution of the cohort showed that no distinct age group was overrepresented (Figure 2A). Plotting of the ΔC_T values and subsequent Pearson correlation testing for the *IRX1*, *EGR3*, and *ICOSLG* expressions revealed that the *ICOSLG* expression strongly correlated with the expression of *EGR3* and *IRX1* (Figures 2B–2F). The highest Pearson R value for the *EGR3-ICOSLG* relation (Figure 2E) was in line with the observation that EGR3 binds directly to the *ICOSLG* promoter in the SEM cell model system (Figures 1C and 1D). According to our studies, IRX1 does not directly bind the *EGR3* or *ICOSLG* promoter, in agreement with the relatively lower Pearson r values for these correlations (Figures 2D and 2F). In summary, gene expression analysis of patient samples verified that IRX1 upregulates EGR3, which subsequently transactivates ICOSLG in infant t(4;11) ALL, as suggested by our SEM::EGR3 cell culture model system.

School of Medicine, Seattle, WA, USA

[12]Lead contact

*Correspondence: rolf.marschalek@em.uni-frankfurt.de

https://doi.org/10.1016/j.isci.2022.104613

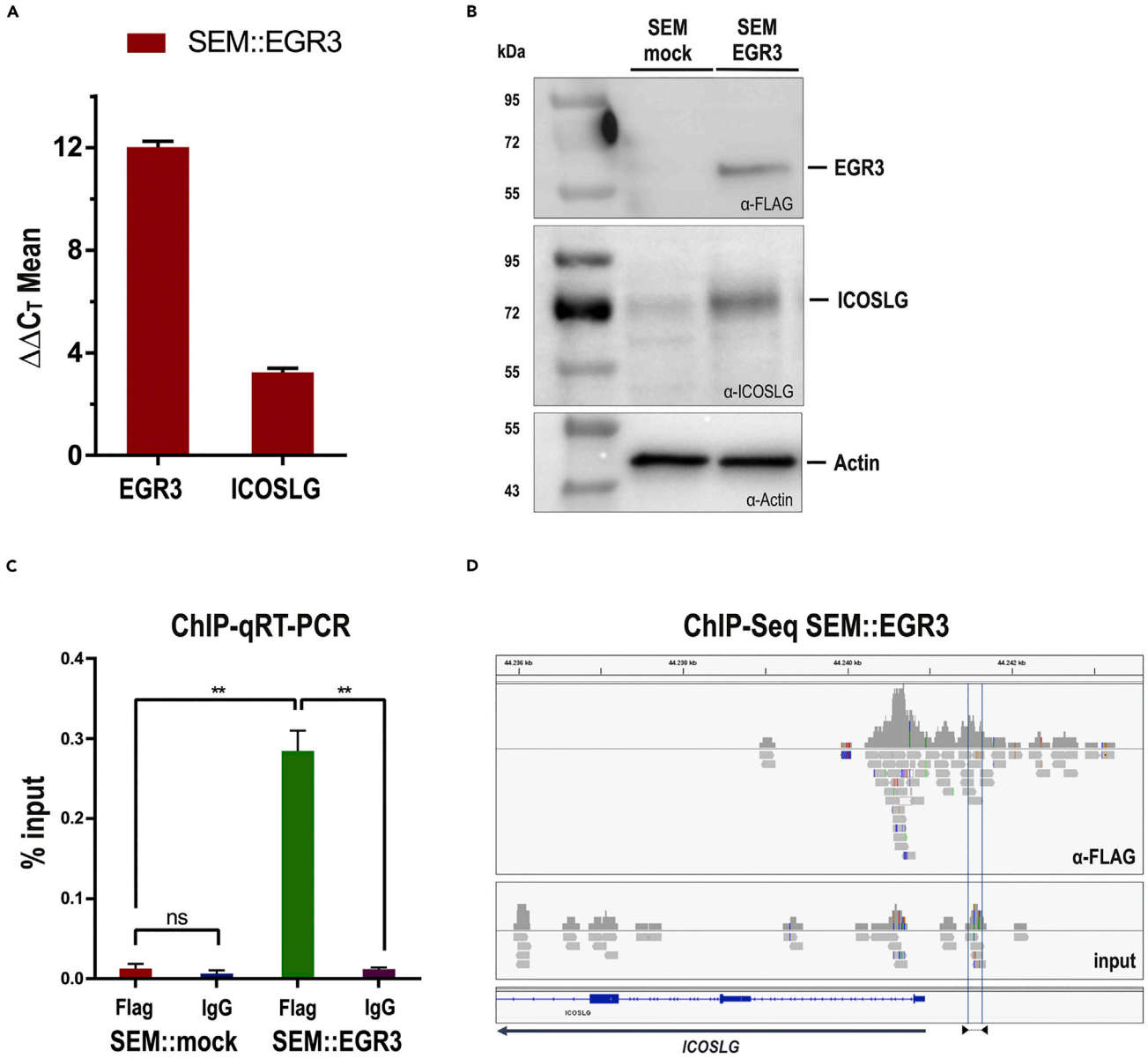

Figure 1. EGR3 upregulates ICOSLG through direct promoter binding in an EGR3-overexpressing t(4;11) SEM cell model

(A) qRT-PCR proved the transcriptional upregulation of EGR3 ($\Delta\Delta C_T$ = 12.03 ± 0.22) and ICOSLG ($\Delta\Delta C_T$ = 3.24 ± 0.16) 48h after the transgene induction of the SEM::EGR3 cell model.

(B) Western blotting of 20 μg protein lysate confirmed the upregulation of EGR3 (FLAG-tagged) and ICOSLG on the protein level. SEM::mock showed a slight ICOSLG band owing to the basal expression of ICOSLG on SEM cells.

(C and D) Chromatin immunoprecipitation followed by qRT-PCR (C) and sequencing (D) displayed the direct binding of EGR3 towards the *ICOSLG* promoter area. ChIP-qRT-PCR was analyzed through percent input calculation followed by two-tailed unpaired *t* tests with Welch's correction to compare the percent input values of SEM:EGR3 α-FLAG with SEM::EGR3 IgG (p = 0.0082), SEM::mock α-FLAG with SEM::mock IgG (p = 0.4452), and SEM::mock α-FLAG with SEM::EGR3 α-FLAG (p = 0.0063). The location of the primer pair used for ChIP-qRT-PCR is displayed as blue lines in the *ICOSLG* promoter area and indicated below with triangles accordingly.

Patients with *HOXA9*^{lo} show slightly inferior EFS than patients with *HOXA9*^{hi} in a cohort of 43 infant patients with t(4;11) pro-B ALL

Patients with t(4;11) iALL were reported to cluster into a *HOXA*^{hi} and a *HOXA*^{lo} group (Trentin et al., 2009), with higher relapse rates in the *HOXA*^{lo} group (Stam et al., 2010; Kang et al., 2012; Symeonidou and Ottersbach, 2021). We aimed to verify this finding and could demonstrate the clustering of patients with t(4;11)

Table 1. Patient characteristics of the dx cohort (n = 50)

Patient no.	Patient age [months]	Treatment protocol	sex	Time to event (last follow-up) [months]	*HOXA9* ΔC_T Mean	*IRX1* ΔC_T Mean	*EGR3* ΔC_T Mean	*ICOSLG* ΔC_T Mean
1	5.0	Interfant-06	F	(40.1)	13.3592	6.1705	8.1850	7.6499
2	6.0	/	F	/	3.9204	7.7667	11.2758	8.0223
3	2.0	Interfant-06	F	(23.6)	12.9546	7.1581	9.3618	7.1255
4	6.0	Interfant-06	M	(17.1)	11.5783	7.9774	11.1637	7.8868
5	10.0	/	M	/	3.5974	8.3317	8.8214	6.0364
6	2.0	Interfant-06	M	(83.6)	4.9698	9.5555	11.5618	6.8416
7	3.0	Interfant-06	F	(5.6)	11.0093	5.1167	8.5196	5.6658
8	3.0	Interfant-06	F	(1.2)	4.9163	6.4184	8.2271	4.8055
9	3.0	Interfant-06	M	(2.5)	4.5976	9.0338	8.0114	9.8380
10	6.0	Interfant-06	F	9.5 (10.7)	5.0818	8.4812	12.3136	9.3984
11	0.1	/	F	/	8.6964	8.0250	11.2989	9.9469
12	1.0	/	M	/	12.3443	6.0576	11.6236	8.4245
13	12.0	/	F	/	2.2824	7.9734	9.1826	7.9894
14	4.0	/	F	/	11.4825	6.3166	11.4695	9.0590
15	2.0	Interfant-06	M	6.0 (6.0)	4.6973	5.9447	13.3440	8.7451
16	5.5	Interfant-06	M	9.5 (15.0)	6.2129	6.5399	9.5330	8.2498
17	1.5	Interfant-06	F	10.0 (13.0)	6.0703	4.9900	6.2132	4.0517
18	3.0	Interfant-06	F	6.0 (11.5)	2.0906	8.4791	9.4723	8.5023
19	2.0	Interfant-06	F	10.5 (19)	7.8537	3.1429	7.2056	5.2518
20	1.5	Interfant-06	M	26.5 (41.0)	4.4627	8.3685	11.2026	7.5564
21	6.5	Interfant-06	M	24.0 (32.8)	11.2673	5.3156	8.7817	8.6026
22	6.0	Interfant-06	F	19.5 (23.5)	11.5891	7.0636	10.0553	7.8697
23	12.0	Interfant-06	F	32.0 (60.6)	11.1226	4.2582	8.0600	7.3822
24	9.0	Interfant-06	M	(84.9)	8.7665	2.2034	7.0569	5.8906
25	2.0	Interfant-06	F	(118.8)	4.6017	7.1138	10.2925	7.1171
26	3.0	Interfant-06	M	8.0 (108.5)	13.0872	5.9083	8.7375	8.5604
27	5.5	Interfant-06	M	(9.0)	5.9626	8.1536	9.1105	8.6464
28	5.0	Interfant-06	M	17.0 (33.0)	5.9922	4.8934	5.0456	3.8081
29	2.0	Interfant-06	F	56.0 (58.6)	5.3297	8.4461	9.3271	8.9127
30	1.5	Interfant-06	F	(146.1)	5.8358	8.0518	9.8910	8.1978
31	8.3	Interfant-06	F	(109.3)	2.2195	6.2132	6.5075	6.2880
32	8.2	Interfant-06	M	(95.9)	1.7726	7.4956	7.2074	7.4143
33	10.7	Interfant-06	M	8.8 (8.8)	2.6953	3.0935	2.4138	4.9064
34	1.7	Interfant-06	F	(91.5)	3.8579	7.1200	6.2540	7.6448
35	11.7	Interfant-06	F	(73.2)	2.9311	7.9152	10.9273	7.2855
36	10.4	Interfant-06	F	(75.9)	5.7541	8.8581	10.4144	9.1282
37	2.4	Interfant-06	F	(73.8)	13.3331	6.1426	9.8438	9.0200
38	4.5	Interfant-06	M	16.1 (63.5)	4.6562	8.9152	11.4891	8.7484
39	1.1	Interfant-06	F	3.3 (15.7)	12.9071	6.3552	11.9464	9.3496
40	5.3	Interfant-06	M	(58.7)	5.4284	8.4380	10.3705	8.3493
41	6.9	Interfant-06	F	(63.2)	9.2472	8.5374	9.7053	6.0532
42	5.3	Interfant-06	M	(60.7)	3.4737	7.4371	9.5640	7.1599
43	0.6	Interfant-06	F	5.0 (11.9)	7.9122	6.2711	8.6364	8.0174

(*Continued on next page*)

Table 1. *Continued*

Patient no.	Patient age [months]	Treatment protocol	sex	Time to event (last follow-up) [months]	*HOXA9* ΔC_T Mean	*IRX1* ΔC_T Mean	*EGR3* ΔC_T Mean	*ICOSLG* ΔC_T Mean
44	1.5	Interfant-06	M	17.3 (18.3)	8.1333	8.0008	9.5745	7.1672
45	4.4	Interfant-06	M	6.6 (10.8)	4.2993	8.0016	10.2528	8.4346
46	9.1	Interfant-06	F	39.7 (45.2)	3.1663	7.7915	9.3985	8.2159
47	0.5	Interfant-06	F	8.7 (13.3)	6.2701	6.5276	9.9358	7.8396
48	6.1	AIEOP-BFM ALL 2017	F	6.6	12.6734	4.2609	9.4741	4.7534
49	6.1	AIEOP-BFM ALL 2017	F	8.3	4.5847	8.1496	10.5529	7.6922
50	10.6	/	M	/	5.0774	9.4705	5.1199	5.4875

All samples were taken from PB at the day of diagnosis. Gene expression values are indicated as the ΔCT mean of three technical replicates. F = female, M = male.

iALL into these two subgroups when analyzing the *HOXA9* transcriptional profiles (19 pts with *HOXA9*^{lo}, 31 pts with *HOXA9*^{hi}). Within the cohort of 50 patients, outcome data were available for 43 pts. We divided the patients into a group that achieved no event within 5 years from diagnosis (n = 12), and a group that achieved an event within the same time frame (n = 23). The assignment of these patients to the respective *HOXA9* transcription level revealed that patients with *HOXA9*^{lo} were found in both groups (Figure 3A). Subsequent Kaplan-Meier analysis of all patients with the availabe outcome data (n = 43) demonstrated that the EFS disadvantage of patients with *HOXA9*^{lo} was quite modest and did not reach statistical significance in a log rank test (Figure 3B). Consistent with the above-mentioned studies, patients with *HOXA9*^{lo} displayed a higher median *IRX1* expression level than patients with *HOXA9*^{hi} (p = 0.0012) (Figure 3C). However, this was not the case for the *EGR3* expression level (p = 0.5397) (Figure 3D) although we showed that the *IRX1* and *EGR3* expressions correlate strongly among the 50 patients (Figure 2D).

High *ICOSLG* expression is associated with inferior EFS in a cohort of 43 infant patients with t(4;11) pro-B ALL

We then focused on *ICOSLG* expression, hypothesizing it could contribute to therapy resistance and relapse rates. For that purpose, we assigned the patients of the "no event group" (n = 12) and the "event group" (n = 23) to their respective *ICOSLG* transcription levels and found the clustering of patients into an *ICOSLG*^{lo} and an *ICOSLG*^{hi} group (Figure 4A). Interestingly, the "no event group" consisted only of patients with *ICOSLG*^{lo}, whereas the "event group" included an *ICOSLG*^{lo} and an *ICOSLG*^{hi} cluster. The Kaplan-Meier analysis of all patients with available outcome data (n = 43) clearly demonstrated inferior EFS of the *ICOSLG*^{hi} group (n = 7; 2-year-EFS = 0.0%) compared to the *ICOSLG*^{lo} group (n = 36; 2-year-EFS = 58.8 $\pm$ 8.5%) (Figure 4B). A log rank test confirmed that both curves were significantly different (p value = 0.0107). However, this analysis could be biased owing to the difference in group sizes, but was not biased owing to patient age as the *ICOSLG*^{hi} group is composed of patients younger and older than 6 months (Figure 4C). In agreement with our previous data, we showed that the *ICOSLG*^{hi} group (n = 8) of all patients (n = 50) possessed significantly elevated *IRX1* and *EGR3* transcription levels. (Figures 4D and 4E).

High *EGR3* and *ICOSLG* expressions are relapse associated

To examine whether the high expression of *ICOSLG* at diagnosis could be associated with relapse formation, we assessed the *HOXA9*, *IRX1*, *EGR3,* and *ICOSLG* gene expressions in a cohort of 18 relapsed pro-B iALL patient samples with different *KMT2A*-r partner genes taken at the time of relapse. These patients were an independent cohort, not related to the samples taken at diagnosis and patient characteristics are summarized in Table 2. We compared the gene expression data of the cohort at initial diagnosis ("dx") with that one at relapse diagnosis ("rel"). To enable an appropriate comparison of both groups, we included only those patients of the dx cohort that achieved an event (n = 23). Thereby, we found that the rel cohort possessed a generally higher expression level of *EGR3* and *ICOSLG* when compared to the dx cohort (Figure 5A). Notably, the *ICOSLG* expression of the rel cohort was mainly at the same level as the *ICOSLG*^{hi} group of the dx cohort (Figure 5B). The higher *EGR3* and *ICOSLG* expressions of the rel cohort compared to the dx cohort were statistically significant in unpaired *t* tests (p < 0.0001) (Figures 5B and 5C), whereas no clear difference became obvious regarding the *IRX1* and *HOXA9* expression comparison of both cohorts (Figures 5D and 5E). Subsequently, we performed a principal component

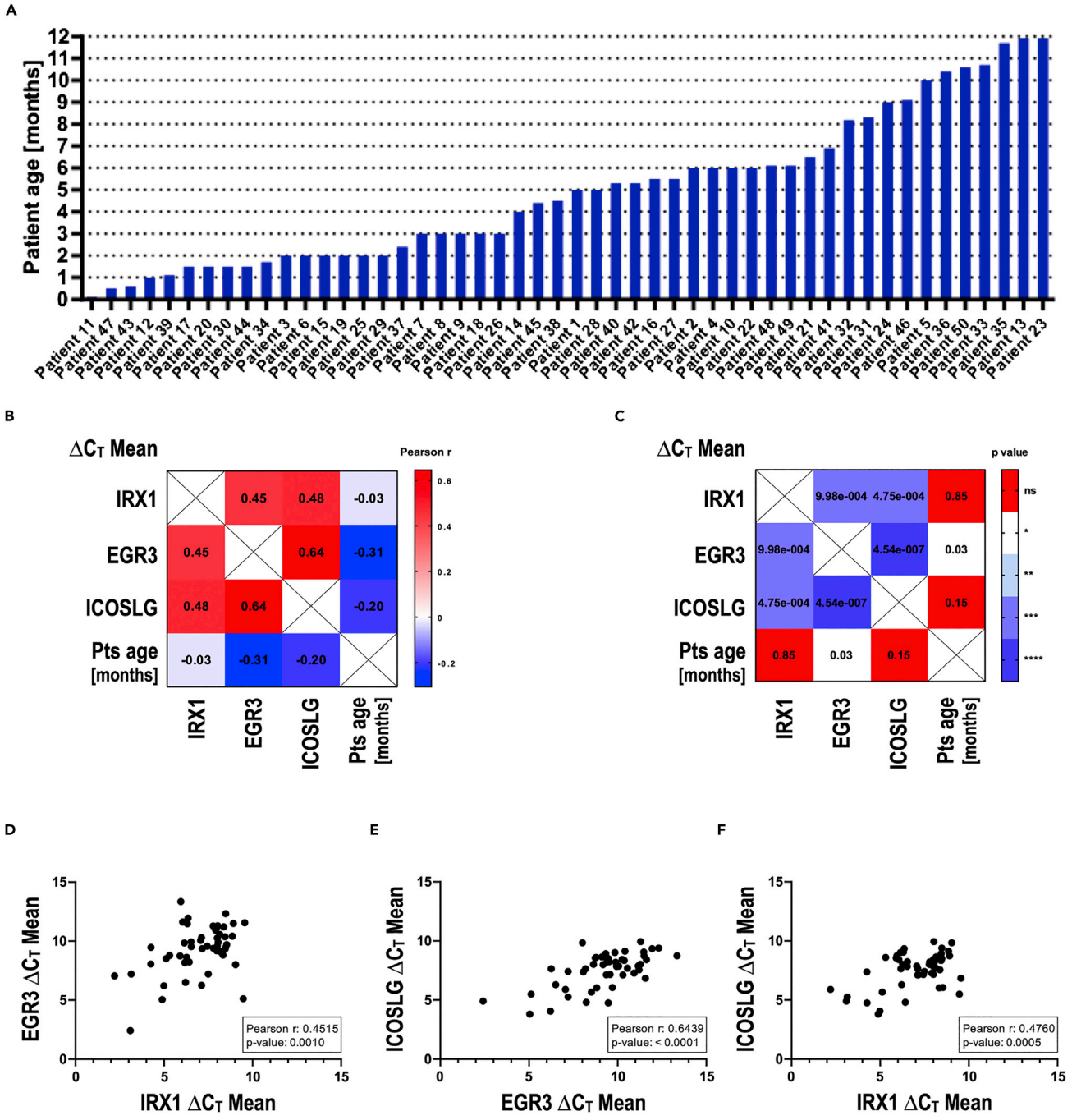

Figure 2. *IRX1*, *EGR3*, and *ICOSLG* expressions correlate strongly in a cohort of 50 infant patients with t(4;11) pro-B ALL

(A) Patient age distribution. Patients of all infant age groups are represented, and no age group is overrepresented.

(B–F) Pearson correlation matrix visualizes the Pearson r values (B) and corresponding p values (C) for all correlations tested. The strong positive correlations between the expressions of *EGR3*-> *IRX1* (D), *ICOSLG*-> *EGR3* (E) and *ICOSLG*-> *IRX1* (F) are obvious mapping each patient sample in the correlation plots.

analysis (PCA) of the *IRX1*, *EGR3*, and *ICOSLG* expression data of the dx and rel cohorts using ClustVis (Metsalu and Vilo, 2015). Patients were assigned to the dx *ICOSLG*^{hi} group, dx *ICOSLG*^{lo} group, or the rel cohort to display the clustering of the patients representing the grade of similarity of their gene expression profiles (Figure 5F). The dx *ICOSLG*^{hi} group (red) clustered together and overlapped completely with the rel cohort (green), whereas the dx *ICOSLG*^{lo} group (blue) clustered besides with only a marginal overlap. The

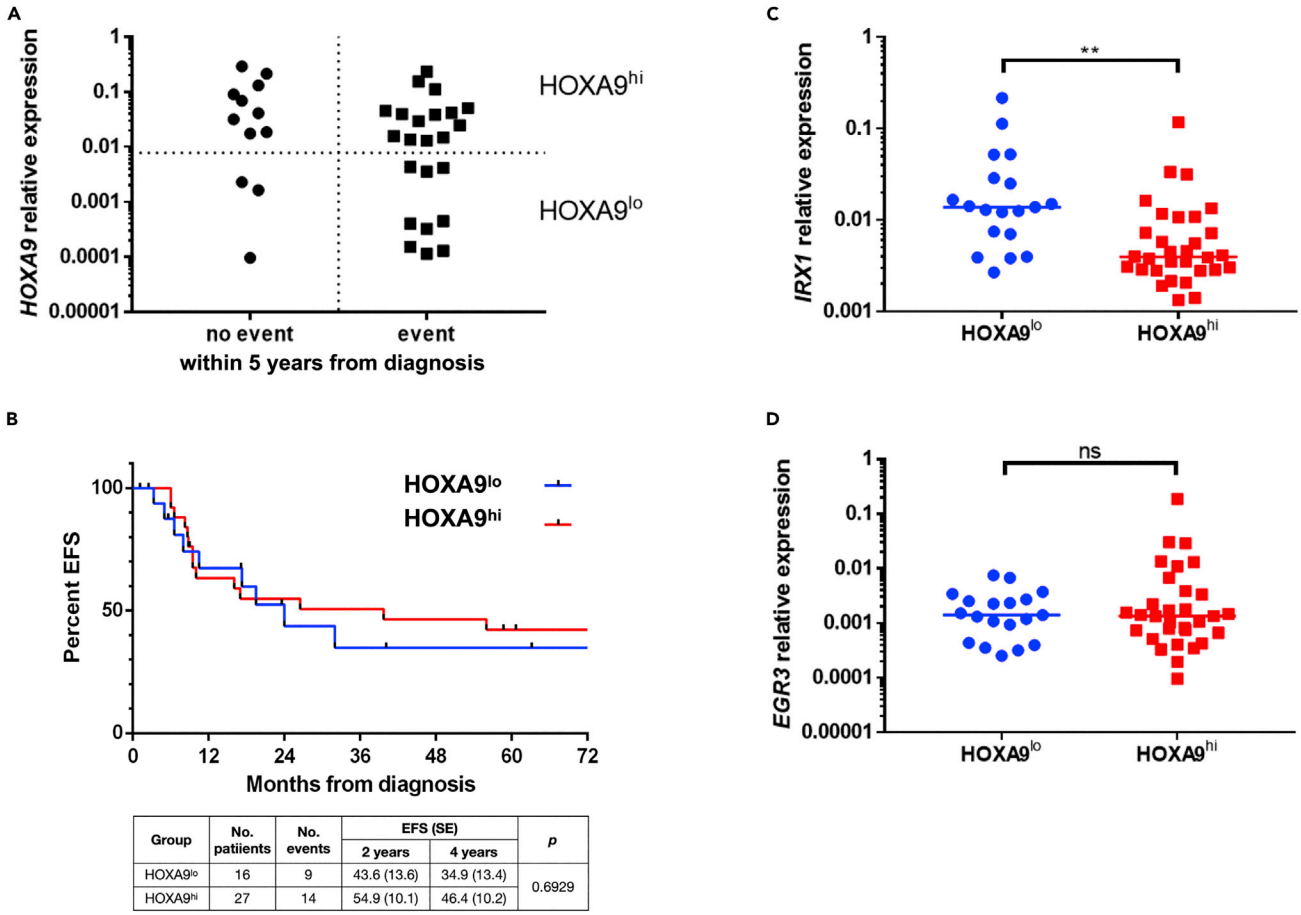

Group	No. patiients	No. events	EFS (SE)		p
			2 years	4 years	
HOXA9lo	16	9	43.6 (13.6)	34.9 (13.4)	0.6929
HOXA9hi	27	14	54.9 (10.1)	46.4 (10.2)	

Figure 3. Patients with *HOXA9*^{lo} show slightly inferior EFS than patients with *HOXA9*^{hi} in a cohort of 43 infant patients with t(4;11) pro-B ALL

(A) Patients were divided into a group that displayed no event within 5 years from diagnosis (n = 12), and a group with an event within the same time frame (n = 23). Subsequently, patients were assigned to the respective *HOXA9* transcription level and divided into a *HOXA9*^{lo} and a *HOXA9*^{hi} subgroup.

(B) Kaplan-Meier curves of the patients with *HOXA9*^{lo} vs *HOXA9*^{hi} visualize the slightly inferior EFS of patients with *HOXA9*^{lo} which did not reach statistical significance in a log rank test (p = 0.6929).

(C and D) Patients with *HOXA9*^{lo} have a higher median *IRX1* (p = 0.012) (C) but not *EGR3* gene expression (p = 0.5397) (D) than patients with *HOXA9*^{hi}. Significance was tested with two-tailed unpaired *t* tests.

coherent clustering of the dx *ICOSLG*^{hi} group with the rel cohort against dx *ICOSLG*^{lo} became also obvious regarding the PCA heatmap (Figure 5G). Thus, PCA revealed a high grade of similarity regarding *IRX1*, *EGR3*, and *ICOSLG* expressions between the group of patients with high *ICOSLG* expression at diagnosis and the relapsed cohort. Taken together, these results strongly suggest that the IRX1-EGR3-ICOSLG axis is involved in relapse formation, and that high *ICOSLG* expression level at diagnosis can be described as a predictor for subsequent relapse.

ICOSLG upregulation in SEM::EGR3 cells leads to the rapid development of T_{regs} upon co-culture with primary T-cells

We then speculated that the causal relationship between *ICOSLG* expression and relapse in t(4;11) iALL could be the ICOSLG-mediated induction of T_{reg} development which was previously described in different physiological and pathological contexts (Martin-Orozco et al., 2010; Lee et al., 2017; Han et al., 2018; Iwata et al., 2019). Accordingly, we examined this question in the t(4;11) pro-B cellular context using the established SEM::EGR3 cell line. For this purpose, primary human T-cells were co-cultured with either SEM::EGR3 or SEM::mock cells for 48h (50% SEM cells with 25% $CD4^+$ and 25% $CD8^+$ T-cells). The T-lymphocytes were isolated from peripheral blood mononuclear cells (PBMC) of healthy MHC-unmatched donors and were stimulated with coated α-CD2/-CD3/-CD28 beads for 16h before co-culture. This stimulation mimicked T-cell receptor (TCR) activation, and thus, enabled a TCR-independent immune activation.

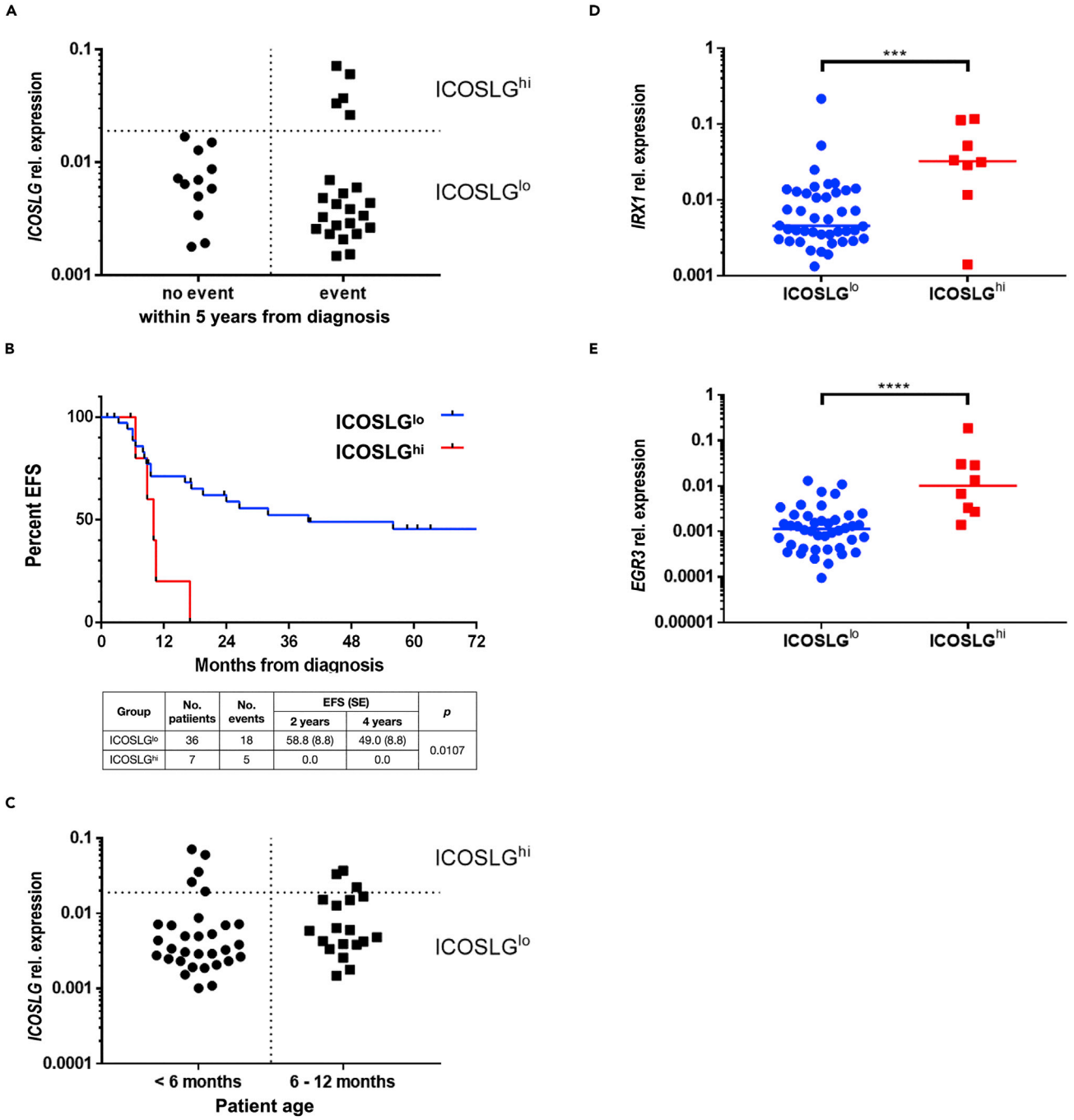

Group	No. patiients	No. events	EFS (SE)		p
			2 years	4 years	
ICOSLG^{lo}	36	18	58.8 (8.8)	49.0 (8.8)	0.0107
ICOSLG^{hi}	7	5	0.0	0.0	

Figure 4. High *ICOSLG* expression is associated with inferior EFS in a cohort of 43 infant patients with t(4;11) pro-B ALL

(A) Patients of the "no event group" (n = 12) and the "event group" (n = 23) were assigned to their respective *ICOSLG* transcription levels and divided into an *ICOSLG*^{lo} and an *ICOSLG*^{hi} subgroup.

(B) Kaplan-Meier curves and log rank test of the patients with *ICOSLG*^{lo} vs *ICOSLG*^{hi} visualize the clearly inferior EFS of patients with *ICOSLG*^{hi} ($p = 0.0107$).

(C) Patients separated by age were assigned to the respective *ICOSLG* transcription level illustrating that the *ICOSLG*^{hi} group was composed of patients younger and older than 6 months.

(D and E) The *ICOSLG*^{hi} group (n = 8) of all patients (n = 50) displayed significantly elevated *IRX1* ($p = 0.0006$) (D) and *EGR3* ($p < 0.0001$) (E) transcription levels in two-tailed unpaired *t* tests.

Table 2. Patient characteristics of the rel cohort (n = 18)

Patient no.	Age at primary diagnosis [months]	KMT2A-r partner	sex	*HOXA9* ΔC_T Mean	*IRX1* ΔC_T Mean	*EGR3* ΔC_T Mean	*ICOSLG* ΔC_T Mean
REZ1	1.3	AFF1	F	2.016418	5.156435	2.832994	6.612465
REZ2	2.9	MLLT1	M	5.517492	6.952302	4.17735	7.647544
REZ3	3.8	AFF1	F	10.23312	2.528003	4.301431	5.388622
REZ4	2.5	AFF1	F	7.767597	2.621157	6.657438	4.662416
REZ5	1.2	AFF1	F	3.034274	6.716536	1.18892	5.421249
REZ6	10.7	MLLT1	M	7.759405	4.871906	5.178097	5.714579
REZ7	4.3	MLLT1	M	−0.47106	4.344864	3.729839	2.899311
REZ8	3.6	MLLT3	F	6.206228	6.106342	4.742364	5.892561
REZ9	9.1	AFF1	F	10.72401	4.103871	2.276168	4.287584
REZ10	0.7	AFF1	F	8.609946	2.540371	1.63076	4.492456
REZ11	4.4	AFF1	M	3.047612	5.159082	6.565317	4.748623
REZ12	4.2	AFF1	M	1.789008	6.10047	5.030182	5.842515
REZ13	2.0	AFF1	F	10.53802	1.708041	2.584866	5.500404
REZ14	3.1	AFF1	F	11.73027	9.246894	8.439681	4.853207
REZ15	7.6	AFF1	F	7.390529	6.94658	7.833634	2.701138
REZ16	6.7	AFF1	M	7.300869	9.940318	9.541564	4.663118
REZ17	5.3	AFF1	M	4.871099	8.645488	9.86666	3.962195
REZ18	7.2	AFF1	M	14.54123	9.570634	6.724747	3.354452

All samples were taken from PB on the day of relapse diagnosis. Gene expression values are indicated as the ΔC_T mean of three technical replicates. F = female, M = male

After 48h of co-culture, the percentage of $CD4^+CD25^+FOXP3^+$ cells (T_{regs}) among $CD4^+$ cells was quantified using flow cytometry. With six independent healthy donors (HD1-6), we observed an increase in the percentage of $CD4^+CD25^+FOXP3^+$ T_{regs} in the SEM::EGR3 co-culture between 7.96 and 23.94% (geometric mean: 1.14 $\pm$ 0.009991, p value = 0.0023) compared to the SEM::mock co-culture (Figure 6B). Noteworthy, SEM::mock cells expressed low amounts of ICOSLG but were not ICOSLG-negative (see Figure 1B).

To prove whether the ICOSLG/ICOS interaction was responsible for T_{reg} development, we performed the experiment under the addition of 20 μg/mL mouse IgG1 isotype control or neutralizing monoclonal mouse α-human ICOSLG antibody to the media (HD1-3). α-ICOSLG but not IgG control antibody impaired the EGR3-mediated T_{reg} development during co-culture. (Figure 6C). These experimental observations suggest that EGR3-expressing t(4;11) ALL cells rapidly induced the development of T_{regs}. This induction was most likely caused by the EGR3-mediated transactivation of *ICOSLG*, as the effect was not observed when the immune checkpoint was selectively blocked by a specific checkpoint inhibitor antibody. We also assessed the cytokine levels in the supernatant of the co-culture using appropriate ELISA tests. These experiments revealed that ICOSLG blockade strongly decreased the IL-10 level of both the SEM::mock and SEM::EGR3 co-culture, whereas the IL-2 levels were not affected (Figures 6D and 6E). All this indicated that ICOSLG blockade impaired the development of T_{regs}. However, for HD1 and HD3 we observed also a strong increase of T_{regs} in the SEM::mock co-culture through ICOSLG antibody blockade which anyway did not affect the decreased IL-10 level through ICOSLG blockade.

T_{regs} exhibit a higher ICOS surface expression than other $CD4^+$ cells after co-culture

We hypothesized that a higher ICOS surface expression on T_{regs} compared to other T-cell subsets could be the reason for the preferential induction of T_{regs} through ICOSLG expression. This has already been reported for T_{regs} in the PB of healthy individuals (Duhen et al., 2012). Flow cytometry analyses revealed that $CD25^+FOXP3^+$ cells displayed a higher ICOS surface expression than $CD25^+FOXP3^-$ and $CD25^-FOXP3^-$ cells within the $CD4^+$ subset (Figure 7). This was neither influenced by the co-cultured cell model (SEM::mock vs SEM::EGR3) nor by different antibody treatments (IgG vs α-ICOSLG). As a result, the higher ICOS surface expression of T_{regs} in comparison to other T-cell subsets was likely the explanation for the induction of T_{regs} through ICOSLG expression.

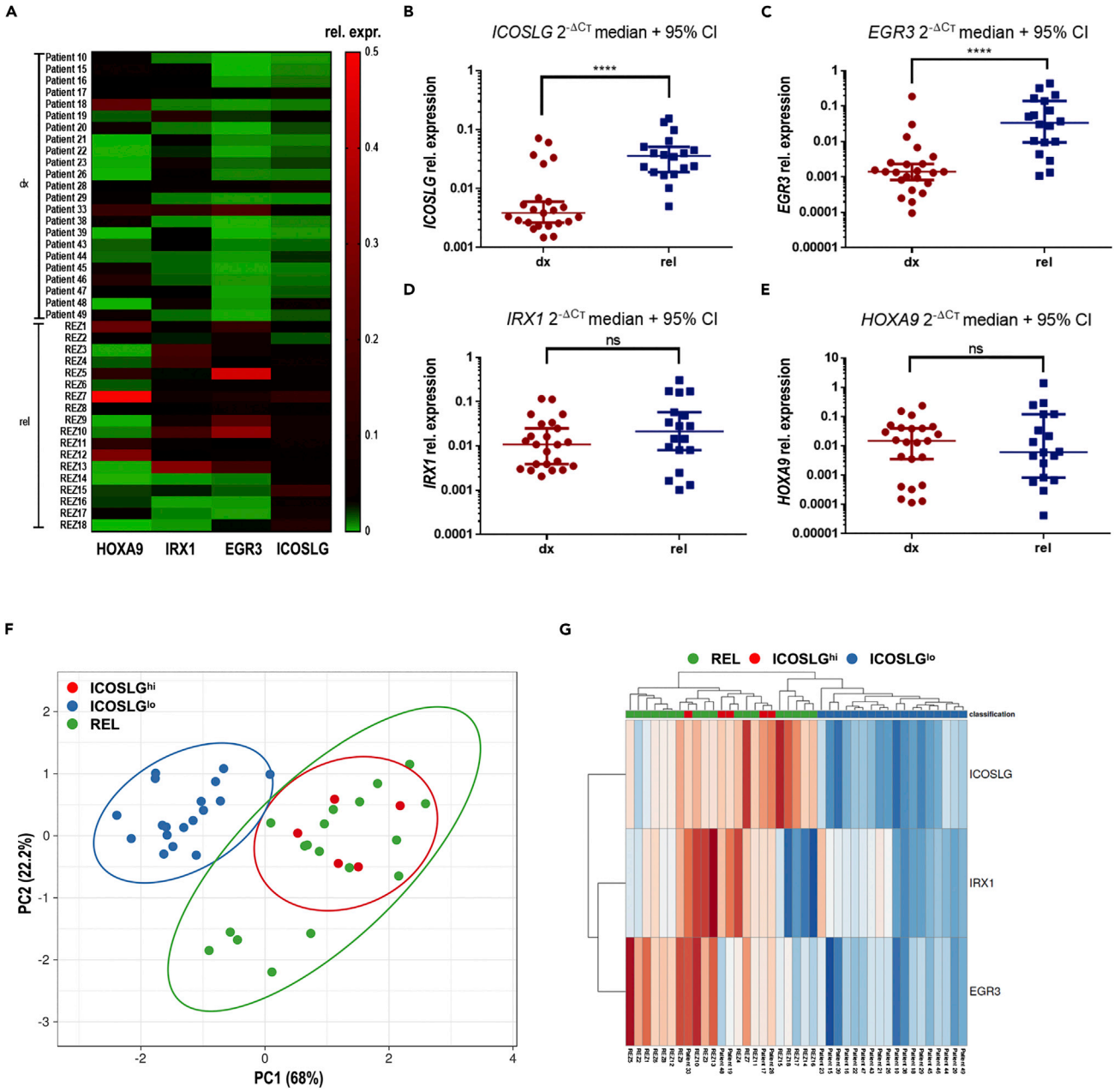

Figure 5. High *EGR3* and *ICOSLG* expressions are relapse associated

(A) *HOXA9*, *IRX1*, *EGR3*, and *ICOSLG* expression levels are displayed in a heatmap for the dx cohort (patients with event; n = 23) and the rel cohort (n = 18). High $2^{-\Delta CT}$ values indicating high expression are displayed in red.

(B–D) Unpaired *t* tests indicated significantly higher *ICOSLG* ($p < 0.0001$) (B) and *EGR3* ($p < 0.0001$) (C) expression levels of the rel cohort compared to the dx cohort, whereas the *HOXA9* and *IRX1* expression levels did not significantly differ between both cohorts ($p_{HOXA9} = 0.8374$; $p_{IRX1} = 0.2737$) (E and D).

(F) Principal component analysis among *IRX1*, *EGR3*, and *ICOSLG* expression data with patients assigned to the rel cohort (green), or to the *ICOSLG*^{hi} (red) or *ICOSLG*^{lo} (blue) group of the dx cohort. PC1 represents 68%, PC2 22.2% of total variance, respectively.

(G) Heatmap of the PCA confirms the clustering of the *ICOSLG*^{hi} group at diagnosis with the relapse cohort. High $2^{-\Delta CT}$ values indicating high transcription levels are displayed in red.

DISCUSSION

Infant t(4;11) ALL is one of the cancers with the lowest mutational burden with approximately 1.3 non-silent mutations in the dominant leukemic clone besides the chromosomal translocation (Andersson et al., 2015; Agraz-Doblas et al., 2019; Brown et al., 2019). Secondary mutations are present in some patients at

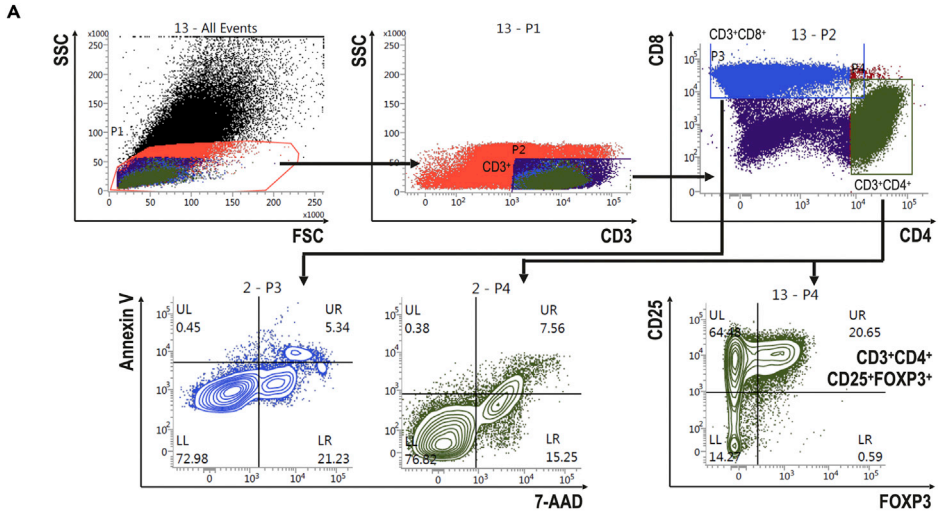
A
13 - All Events
SSC
FSC
P1
13 - P1
CD3+
CD3
13 - P2
CD3+CD8+
CD8
CD4
CD3+CD4+
2 - P3
Annexin V
7-AAD
UL 0.45
UR 5.34
LL 72.98
LR 21.23
2 - P4
UL 0.38
UR 7.56
LR 15.25
13 - P4
CD25
FOXP3
UR 20.65
CD3+CD4+
CD25+FOXP3+
LR 0.59

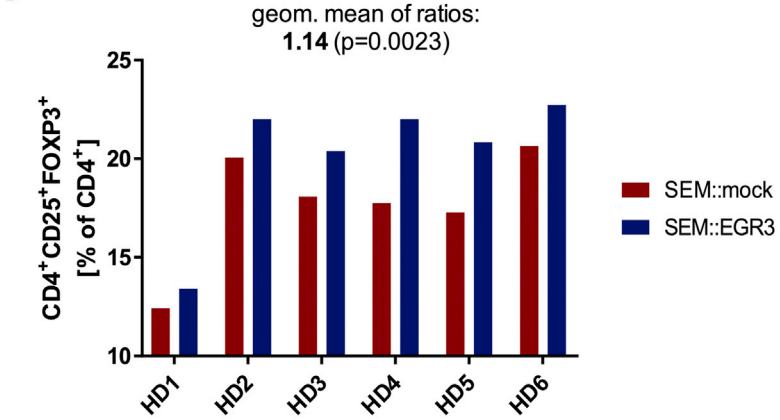
B
geom. mean of ratios:
1.14 (p=0.0023)
CD4+CD25+FOXP3+ [% of CD4+]
HD1
HD2
HD3
HD4
HD5
HD6
SEM::mock
SEM::EGR3

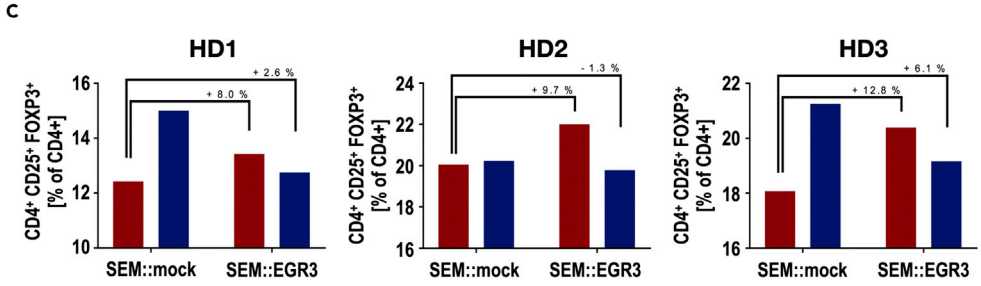
C
HD1
HD2
HD3
CD4+ CD25+ FOXP3+ [% of CD4+]
+ 2.6 %
+ 8.0 %
- 1.3 %
+ 9.7 %
+ 6.1 %
+ 12.8 %
SEM::mock
SEM::EGR3

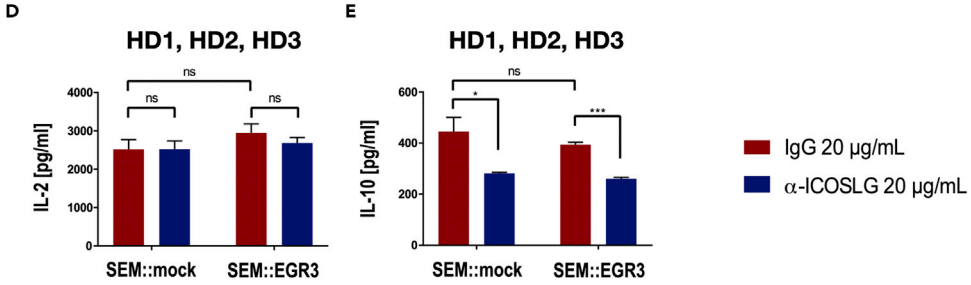
D
HD1, HD2, HD3
IL-2 [pg/ml]
ns
E
HD1, HD2, HD3
IL-10 [pg/ml]
*
***
SEM::mock
SEM::EGR3
IgG 20 µg/mL
α-ICOSLG 20 µg/mL

Figure 6. ICOSLG upregulation in SEM::EGR3 cells leads to the rapid development of T_{regs} upon co-culture with primary T-cells

(A) Flow cytometry gating strategy of the co-cultured cells. Cells with low granularity (low SSC) were gated out of all cells. $CD3^+$ cells were selected to subsequently separate $CD4^+$ and $CD8^+$ cells. Viability after co-culture of these populations was assed using Annexin V and 7-AAD staining to ensure that the majority of T-cells were alive throughout co-culture. $CD25^+FOXP3^+$ cells (T_{regs}) were quantified out of the $CD4^+$ population.

(B) Percentages of $CD4^+CD25^+FOXP3^+$ T_{regs} among $CD4^+$ T-cells after co-culturing T-cells from six healthy donors (HD1-HD6) with SEM::mock or SEM::EGR3. SEM::EGR3 co-culture led to 7.96%-23.94% more T_{regs} than SEM::mock co-culture (geometric mean: 1.14 $\pm$ 0.009991, $p = 0.0023$ in a two-tailed ratio paired *t* test).

(C) Replication of the co-culture experiment of HD1-HD3 under the addition of 20 μg/mL mouse IgG1 isotype control or neutralizing monoclonal mouse α-human ICOSLG antibody demonstrated that EGR3-mediated T_{regs} induction could be impaired through ICOSLG antibody blockade.

(D and E) ELISAs of the co-culture supernatants depicted that ICOSLG antibody blockade has no effect on the IL-2 level (D) but strongly decreased the IL-10 level (SEM::mock: $p = 0.0424$; SEM::EGR3: $p = 0.0002$) (E) of the media. Significance was tested with multiple *t* tests.

diagnosis but are the result of the dramatic cycling activity of the dominant clone and disappear once leukemia re-emerges as a relapse, indicating that the translocation is the only necessary leukemic driver (Agraz-Doblas et al., 2019). Based on our results, we propose that high *ICOSLG* expression at diagnosis and inferior EFS are causally linked, in that the ICOSLG-mediated induction of T_{reg} development counteracts the immune recognition of leukemia cells. Through this mechanism, ALL cells could acquire a protective immune privilege in their bone marrow niche, enabling them to re-emerge as relapse despite ongoing chemotherapy. This mechanism is a possible explanation for relapse occurrence without the accumulation of additional mutations and clonal evolution.

This hypothesis implies that "fusion derived neoantigens" (FDNA) lead to T-cell priming and specific immune responses against the leukemic cells. Although cancers with a low mutational burden are generally regarded as barely immunogenic, *ETV6::RUNX1* fusion-specific $CD8^+$ T-cell responses have been reported in pediatric ALL (Zamora et al., 2019). Moreover, gene fusions are known to render T-cell responses in head and neck tumors with low mutational burden and minimal immune infiltration resulting in clinical response to immune checkpoint blockade (Yang et al., 2019). Therefore, it could be possible that also t(4;11)-derived neoantigens are immunogenic although this has not yet been demonstrated experimentally.

In pediatric ALL, the bone marrow (BM) is the predominant compartment where relapse originates (Tallen et al., 2010; Driessen et al., 2016). The BM provides the specialized niche in which HSC reside and give rise to all subsets of blood cells throughout life (Morrison and Scadden, 2014; Chen et al., 2016). In AML, leukemia stem cells (LSC) occupy the HSC niche and outcompete their healthy counterparts (Bonnet and Dick, 1997; Boyd et al., 2014; Medyouf, 2017; Kumar et al., 2018). In ALL, chemotherapy induces the formation of a protective niche by leukemia-initiating cells (LIC) that perturb hematopoiesis and lead to apoptosis of healthy HSC (Duan et al., 2014; Tang et al., 2018; Burt et al., 2019). In case of t(4;11) ALL, fetal liver-derived $CD34^+CD19^-$ primitive B lineage-negative but lymphoid-restricted progenitor/stem cells have been identified as the most likely cellular origin of transformation (Hotfilder et al., 2005; Rice et al., 2021). However, it has been shown that not only $CD34^+$ but also $CD34^-$ ALL cells including blasts at different stages of differentiation possess stem cell capabilities and may act as LIC when serially transplanted in immunocompromised mice (le Viseur et al., 2008; Aoki et al., 2015). Accordingly, in t(4;11) ALL stemness seems not to be restricted to a certain cell type, suggesting that leukemia cells at different stages of differentiation can home to and reside in the BM niche and subsequently contribute to relapse. Therefore, therapeutic approaches that interfere with leukemic niche formation hold promise to prevent relapse development, particularly in infant t(4;11) ALL.

Importantly, the BM is not only a primary but also a secondary immune organ as it is part of the lymphocyte recirculation network (Osmond, 1994). $CD4^+$ and $CD8^+$ T-cells enter the BM from the vasculature and become primed through BM-residing dendritic cells (DC) resulting in primary immune responses (Feuerer et al., 2001, 2003). Besides $CD4^+$ and $CD8^+$ T-cells, T_{regs} migrate to and accumulate in the BM through CXCL12/CXCR4 interactions (Zou et al., 2004). These T_{regs} have been shown to colocalize with HSC and provide an immune privilege to the niche (Fujisaki et al., 2011). Additionally, niche-associated T_{regs} are known to maintain HSC quiescence (Hirata et al., 2018, 2019). As healthy HSC depend on the colocalization with T_{regs}, it is highly likely that LSC/LIC do as well, considering especially that the recruitment of immune

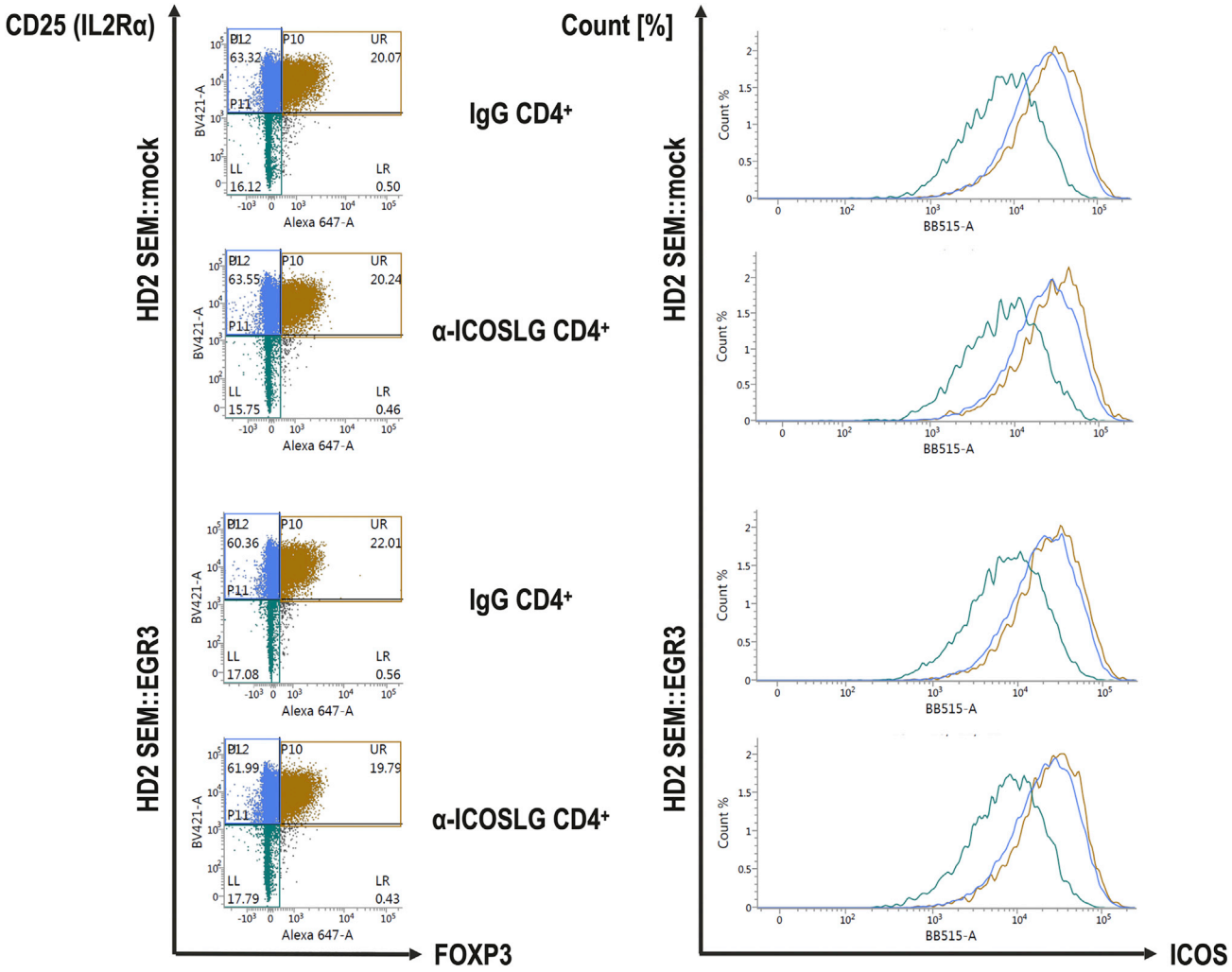

Figure 7. T_{regs} exhibit a higher ICOS surface expression than other $CD4^+$ cells after co-culture

Shown are the representative CD25->FOXP3 dot plots of the $CD3^+CD4^+$ subset of HD2. $CD25^+FOXP3^+$, $CD25^+FOXP3^-$ and $CD25^-FOXP3^-$ cells were gated and their respective ICOS surface expression were displayed in a comparative plot. $CD25^+FOXP3^+$ Tregs showed the highest ICOS expression, followed by $CD25^+FOXP3^-$ cells. $CD25^-FOXP3^-$ cells clearly display the lowest ICOS surface expression.

suppressive cells to avoid immune destruction is a common measure of several solid tumors and a hallmark of cancer (Hanahan and Weinberg, 2011).

Therefore, we speculate that ALL cell expression of ICOSLG facilitates the recruitment of T_{regs} to the BM niche. The ICOSLG/ICOS interaction is known to affect $CD4^+$ T-cells to produce IL-10 resulting in immunosuppression (Figure 8) (Hutloff et al., 1999; Akbari et al., 2002; Löhning et al., 2003). Furthermore, the development of T_{regs} in the healthy bone marrow as well as in melanoma, glioblastoma, breast cancer and AML has been shown to strongly depend on the ICOSLG/ICOS interaction (Martin-Orozco et al., 2010; Faget et al., 2012; Lee et al., 2017; Han et al., 2018; Iwata et al., 2019). Accordingly, the here described identification of EGR3-mediated ICOSLG-expressing ALL cells, enabling increased T_{reg} development is in line with previous observations.

In our study, co-culture of SEM::EGR3 with adult T-cells leads to an enrichment of $ICOS^+FOXP3^+$ T_{regs}. In mice, the high surface expression of ICOS among T_{regs} determines a higher proliferative capability, longer survival, and stronger suppression compared to $ICOS^-$ T_{regs} (Chen et al., 2012). The higher suppressive activity of $ICOS^+$ T_{regs} has also been observed in human studies (Vocanson et al., 2010). ICOS is expressed at low levels in all T-cell subsets but becomes upregulated upon ICOSLG binding (Hutloff et al., 1999;

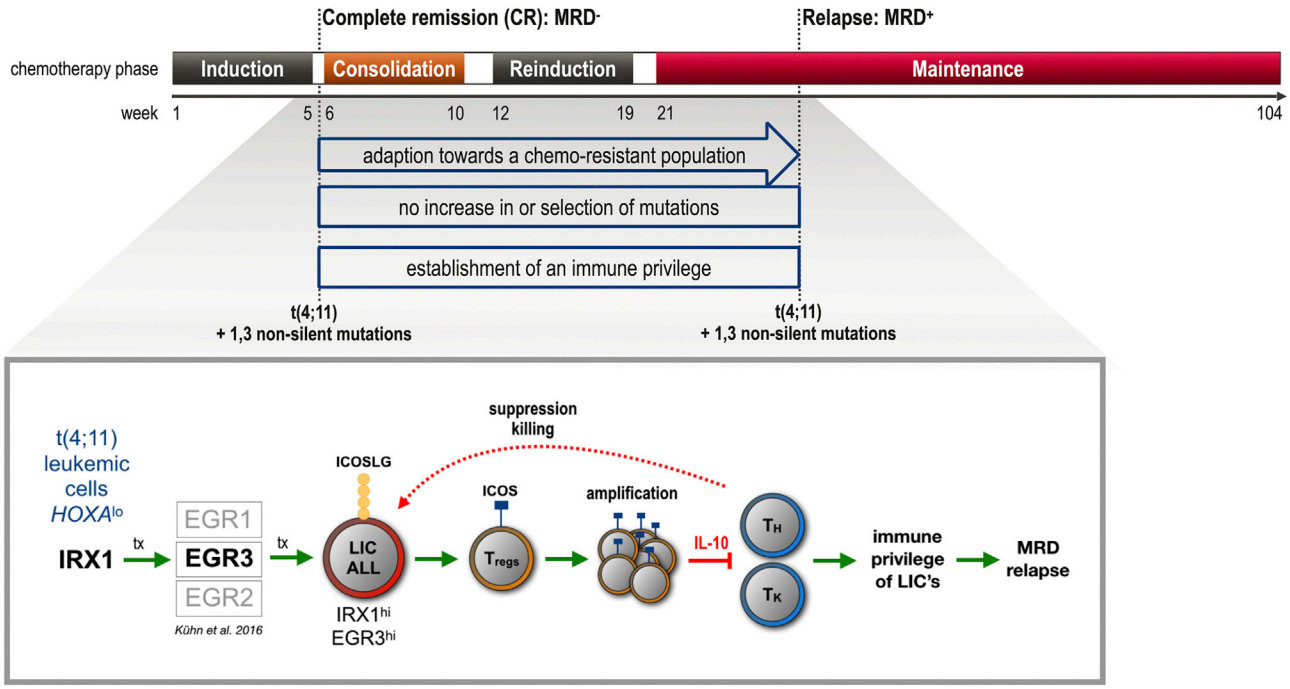

Figure 8. Proposed immune-evasion relapse mechanism in t(4;11) ALL

Upper panel: Scheme of ALL chemotherapy. Although complete remission (CR) is frequently achieved after induction therapy, relapse occurs prevalently during consolidation, reinduction, or maintenance phase. Bottom panel: Infant t(4;11) ALL cells characterized by low *HOXA* transcription overexpress *IRX1*, which in turn causes the upregulation of several EGR transcription factors. EGR3 was shown to cause the transcriptional upregulation of *ICOSLG*. The interaction of ICOSLG on ALL cells with ICOS on T-cells initiates the development of regulatory T-cells (T_{regs}). The accumulation of T_{regs} in the bone marrow niche could provide ALL cells with an immune privilege allowing them to acquire therapy resistance and to develop minimal residual disease (relapse).

Khayyamian et al., 2002). The T_{regs} which developed in our co-culture setting showed the highest ICOS surface expression among the $CD4^+$ T-cells mirroring the results of previous studies (Duhen et al., 2012). Therefore, we assume that the higher and constitutional ICOS surface expression of T_{regs} compared to non-T_{regs} could be a reason for their preferential proliferation during their co-culture with ICOSLG-expressing SEM cells. It is known that $ICOS^+$ T_{regs} suppress other T-cells mainly through IL-10 secretion, whereas $ICOS^-$ T_{regs} secrete transforming growth factor-β (TGF-β) leading to weaker immunosuppression (Ito et al., 2008). In concordance, we show that ICOSLG antibody blockade leads to a strong decrease in the IL-10 level of the co-culture media supernatant. Intracellularly, ICOS activation promotes *FOXP3* transcription, and in turn, FOXP3- and NFAT-dependent transactivation of *IL10* and *TGFB1* (Li and Xiong, 2020). Additionally, $ICOS^+FOXP3^+$ T_{regs} play an important role during fetal development and pregnancy as both cord blood and the newborn's thymus already contain $ICOS^+FOXP3^+$ T_{regs} (Takahata et al., 2004; Ito et al., 2008). Furthermore, the newborn's thymus contains more $ICOS^+FOXP3^+$ T_{regs} than adult peripheral blood and these T_{regs} express the thymus emigration marker CD31 which implies that the $ICOS^+$ T_{reg} subset is derived directly from the thymus and does not develop out of $ICOS^-FOXP3^+$ T_{regs} (Takahata et al., 2004; Ito et al., 2008). The presence of $ICOS^+$ T_{regs} during fetal development is of special interest because it has been demonstrated by twin studies that the translocation t(4;11) arises *in utero*. (Gale et al., 1997; Wiemels et al., 1999; Greaves and Wiemels, 2003; Greaves et al., 2003). During pregnancy, the fetus is protected from the mother's semiforeign immune system through placental trophoblast cells which surround fetal tissues. ICOSLG is highly expressed throughout pregnancy by the extravillous trophoblast cells (EVT) (Petroff et al., 2005) and has been validated as a mediator of tolerance at the fetomaternal interface during pregnancy (Riella et al., 2013). Furthermore, EVTs mediate the invasion and differentiation of decidual T_{regs} which suppress T-cell responses during pregnancy through the secretion of IL-10 (Aluvihare et al., 2004; Tilburgs et al., 2008; Du et al., 2014; Svensson-Arvelund et al., 2015; Salvany-Celades et al., 2019). Taken together, it is highly likely that the ICOSLG/ICOS interaction also provides an immune privilege to the fetomaternal interface. Recombining this knowledge with the results of our study leads to the suggestion that t(4;11) iALL depends on an immune privilege firstly to occur *in utero* and secondly to relapse in the BM. Accordingly, the ICOSLG-mediated T_{reg} development in the leukemic BM niche could reflect the immune

privilege during pregnancy, and thus could be a prerequisite for relapse development. Correspondingly, switching the immune-privileged leukemic BM niche toward immune-susceptibility holds promise to prevent relapse or to treat relapse-associated therapy resistance.

Here, we have shown that elevated *ICOSLG* expression at diagnosis is predictive for relapse development, and that targeting ICOSLG with a neutralizing mAb prevents the ICOSLG-mediated T_{reg} induction *in vitro*. Based on these findings, we propose the clinical investigation of ICOSLG targeting therapies such as the α-ICOSLG fully human mAb Prezalumab. Prezalumab (AMG 557/MEDI 5872) has been tested clinically for the treatment of autoimmune diseases such as systemic lupus erythematosus (SLE) and active lupus arthritis in three phase I trials: NCT02391259, NCT00774943, and NCT01683695 (Sullivan et al., 2016; Cheng et al., 2018). In the first and second trial, 112 adult patients with mild SLE were enrolled and the safety and tolerability of single (1.8-210 mg s.c. or 18 mg i.v.) vs. multiple (6-210 mg s.c. every other week) dose administration of Prezalumab have been shown. Importantly, only non-neutralizing α-Prezalumab antibodies were observed. The third trial demonstrated the long-term (23 weeks) safety and tolerability of Prezalumab among 10 patients. However, Prezalumab failed to demonstrate clinical improvement in a phase IIa study (NCT02334306) for the treatment of primary Sjögren's syndrome halting all further clinical investigation (Mariette et al., 2019; Pontarini et al., 2020).

Unfortunately, up to now, no studies were conducted to evaluate the safety of Prezalumab in infants or children with ALL. Regarding checkpoint inhibition in general, an interim analysis is available of the KEYNOTE-051 trial (NCT02332668), a phaseI/II study evaluating the safety and efficacy of Pembrolizumab (α-PD-L1) in children >6 months with advanced melanoma or PD-L1 positive solid tumor or lymphoma (Geoerger et al., 2020). Three patients aged 6 months-2 years, 22 aged 2-5 years, 25 aged 6-9 years, and 104 aged 10-17 years were enrolled. The study proved Pembrolizumab checkpoint inhibition safe in children as serious adverse events occurred only in 9% of patients (pyrexia, hypertension, and pleural effusion). Besides, another phase I/II trial proved the safety and tolerability of the PD-1 checkpoint inhibitor Nivolumab in children >1 year with lymphoma (Davis et al., 2020). These studies demonstrate that PD-1/PD-L1 immune checkpoint inhibition is safe in young children; however, the safety of ICOSLG-directed mAbs remains to be demonstrated in infants and children.

In summary, we provide a molecular rationale for the clinical evaluation of immune-based therapies targeting the ICOSLG/ICOS interaction for the treatment and prevention of relapse in infants with t(4;11) ALL. Further studies are needed to clarify whether t(4;11)-derived neoantigens lead to immune responses in infants and if that explains the potential demand of the disease for an immune-privileged site firstly to originate *in utero* and secondly to relapse in the BM. Even though these questions remain unanswered, we communicate our findings to enable a rapid translation into the clinical investigation.

LIMITATIONS OF THE STUDY

The conclusion of this study has been obtained by *in vitro* studies, and thus, an appropriate mouse model is still missing. Also, the co-culture experiments with genetically modified t(4;11) cells, overexpressing the ICOSLG, were performed *in vitro* with a limited time window (48 h) and without MHC matching. In addition, we used a neutralizing commercial antibody against ICOSLG and not the clinically tested Prezalumab (AMGEN) because this antibody was not available to us.

STAR★METHODS

Detailed methods are provided in the online version of this paper and include the following:

- KEY RESOURCES TABLE
- RESOURCE AVAILABILITY
  - Lead contact
  - Materials availability
  - Data and code availability
- EXPERIMENTAL MODEL AND SUBJECT DETAILS
  - Animals
  - Cell culture
  - Co-culture study

ACKNOWLEDGMENTS

We thank all our collaborators for fruitful discussions and Birthe Fedders for sample composition and sending. This work has been funded in part by DFG grants MA 1876/12-1 and MA 1876/13-1.

AUTHOR CONTRIBUTIONS

MK and RM wrote the article; MK, HB, and RM planned and interpreted experiments; MK generated cell lines, performed qRT-PCR, Western blot, co-culture experiments, flow cytometry and ELISA; ALS performed plasmid cloning; CM, PL, and MK performed ChIP-Seq; CM and PL helped to write the article; AD and MK performed ChIP-qRT-PCR; JA, GC, CE, ACE, HC, MB, GiC, PDL, and MGV provided patient samples and outcome data, and helped to analyze clinical data; LD and HB provided blood samples and contributed to T-cell isolation; RM supervised the study and provided funding; all authors reviewed and approved the article.

DECLARATION OF INTERESTS

The authors declare that they have no competing interests.

Received: March 17, 2022
Revised: April 14, 2022
Accepted: June 1, 2022
Published: July 15, 2022

REFERENCES

Agraz-Doblas, A., Bueno, C., Bashford-Rogers, R., Roy, A., Schneider, P., Bardini, M., Ballerini, P., Cazzaniga, G., Moreno, T., Revilla, C., et al. (2019). Unraveling the cellular origin and clinical prognostic markers of infant B-cell acute lymphoblastic leukemia using genome-wide analysis. Haematologica *104*, 1176–1188. https://doi.org/10.3324/haematol.2018.206375.

Akbari, O., Freeman, G.J., Meyer, E.H., Greenfield, E.A., Chang, T.T., Sharpe, A.H., Berry, G., DeKruyff, R.H., and Umetsu, D.T. (2002). Antigen-specific regulatory T cells develop via the ICOS–ICOS-ligand pathway and inhibit allergen-induced airway hyperreactivity. Nat. Med. *8*, 1024–1032. https://doi.org/10.1038/nm745.

Aluvihare, V.R., Kallikourdis, M., and Betz, A.G. (2004). Regulatory T cells mediate maternal tolerance to the fetus. Nat. Immunol. *5*, 266–271. https://doi.org/10.1038/ni1037.

Anderson, P.O., Manzo, B., Sundstedt, A., Minaee, S., Symonds, A., Khalid, S., Rodriguez-Cabezas, M., Nicolson, K., Li, S., Wraith, D., and Wang, P. (2006). Persistent antigenic stimulation alters the transcription program in T cells, resulting in antigen-specific tolerance. Eur. J. Immunol. *36*, 1374–1385. https://doi.org/10.1002/eji.200635883.

Andersson, A.K., Ma, J., Wang, J., Chen, X., Gedman, A.L., Dang, J., Nakitandwe, J., Holmfeldt, L., Parker, M., Easton, J., et al. (2015). The landscape of somatic mutations in infant MLL-rearranged acute lymphoblastic leukemias. Nat. Genet. *47*, 330–337. https://doi.org/10.1038/ng.3230.

Aoki, Y., Watanabe, T., Saito, Y., Kuroki, Y., Hijikata, A., Takagi, M., Tomizawa, D., Eguchi, M., Eguchi-Ishimae, M., Kaneko, A., et al. (2015). Identification of CD34+ and CD34− leukemia-initiating cells in MLL-rearranged human acute lymphoblastic leukemia. Blood *125*, 967–980. https://doi.org/10.1182/blood-2014-03-563304.

Bonnet, D., and Dick, J.E. (1997). Human acute myeloid leukemia is organized as a hierarchy that originates from a primitive hematopoietic cell. Nat. Med. *3*, 730–737. https://doi.org/10.1038/nm0797-730.

Boyd, A.L., Campbell, C.J., Hopkins, C.I., Fiebig-Comyn, A., Russell, J., Ulemek, J., Foley, R., Leber, B., Xenocostas, A., Collins, T.J., and Bhatia, M. (2014). Niche displacement of human leukemic stem cells uniquely allows their competitive replacement with healthy HSPCs. J. Exp. Med. *211*, 1925–1935. https://doi.org/10.1084/jem.20140131.

Brown, P., Pieters, R., and Biondi, A. (2019). How I treat infant leukemia. Blood *133*, 205–214. https://doi.org/10.1182/blood-2018-04-785980.

Burt, R., Dey, A., Aref, S., Aguiar, M., Akarca, A., Bailey, K., Day, W., Hooper, S., Kirkwood, A., Kirschner, K., et al. (2019). Activated stromal cells transfer mitochondria to rescue acute lymphoblastic leukemia cells from oxidative stress. Blood *134*, 1415–1429. https://doi.org/10.1182/blood.2019001398.

Chen, Y., Shen, S., Gorentla, B.K., Gao, J., and Zhong, X.P. (2012). Murine regulatory T cells contain hyperproliferative and death-prone subsets with differential ICOS expression. J. Immunol. *188*, 1698–1707. https://doi.org/10.4049/jimmunol.1102448.

Chen, J.Y., Miyanishi, M., Wang, S.K., Yamazaki, S., Sinha, R., Kao, K.S., Seita, J., Sahoo, D., Nakauchi, H., and Weissman, I.L. (2016). Hoxb5 marks long-term haematopoietic stem cells and reveals a homogenous perivascular niche. Nature

530, 223–227. https://doi.org/10.1038/nature16943.

Cheng, H., Hao, S., Liu, Y., Pang, Y., Ma, S., Dong, F., Xu, J., Zheng, G., Li, S., Yuan, W., and Cheng, T. (2015). Leukemic marrow infiltration reveals a novel role for Egr3 as a potent inhibitor of normal hematopoietic stem cell proliferation. Blood *126*, 1302–1313. https://doi.org/10.1182/blood-2015-01-623645.

Cheng, L.E., Amoura, Z., Cheah, B., Hiepe, F., Sullivan, B.A., Zhou, L., Arnold, G.E., Tsuji, W.H., Merrill, J.T., and Chung, J.B. (2018). Brief report: a randomized, double-blind, parallel-group, placebo-controlled, multiple-dose study to evaluate AMG 557 in patients with systemic lupus erythematosus and active lupus arthritis. Arthritis Rheumatol. *70*, 1071–1076. https://doi.org/10.1002/art.40479.

Collins, S., Lutz, M., Zarek, P., Anders, R., Kersh, G., and Powell, J. (2008). Opposing regulation of T cell function by Egr-1/NAB2 and Egr-2/Egr-3. Eur. J. Immunol. *38*, 528–536. https://doi.org/10.1002/eji.200737157.

Coyle, A.J., and Gutierrez-Ramos, J.C. (2001). The expanding B7 superfamily: increasing complexity in costimulatory signals regulating T cell function. Nat. Immunol. *2*, 203–209. https://doi.org/10.1038/85251.

Davis, K.L., Fox, E., Merchant, M.S., Reid, J.M., Kudgus, R.A., Liu, X., Minard, C.G., Voss, S., Berg, S.L., Weigel, B.J., and Mackall, C.L. (2020). Nivolumab in children and young adults with relapsed or refractory solid tumours or lymphoma (ADVL1412): a multicentre, open-label, single-arm, phase 1–2 trial. Lancet Oncol. *21*, 541–550. https://doi.org/10.1016/S1470-2045(20)30023-1.

Driessen, E.M.C., de Lorenzo, P., CaMpbell, M., Felice, M., Ferster, A., Hann, I., VorA, A., Hovi, L., Escherich, G., Li, C.K., et al. (2016). Outcome of relapsed infant acute lymphoblastic leukemia treated on the interfant-99 protocol. Leukemia *30*, 1184–1187. https://doi.org/10.1038/leu.2015.246.

Du, M.-R., Guo, P.F., Piao, H.L., Wang, S.C., Sun, C., Jin, L.P., Tao, Y., Li, Y.H., Zhang, D., Zhu, R., et al. (2014). Embryonic trophoblasts induce decidual regulatory T cell differentiation and maternal–fetal tolerance through thymic stromal lymphopoietin instructing dendritic cells. J. Immunol. *192*, 1502–1511. https://doi.org/10.4049/jimmunol.1203425.

Duan, C.-W., Shi, J., Chen, J., Wang, B., Yu, Y.H., Qin, X., Zhou, X.C., Cai, Y.J., Li, Z.Q., Zhang, F., et al. (2014). Leukemia propagating cells rebuild an evolving niche in response to therapy. Cancer Cell *25*, 778–793. https://doi.org/10.1016/j.ccr.2014.04.015.

Duhen, T., Duhen, R., Lanzavecchia, A., Sallusto, F., and Campbell, D.J. (2012). Functionally distinct subsets of human FOXP3+ Treg cells that phenotypically mirror effector Th cells. Blood *119*, 4430–4440. https://doi.org/10.1182/blood-2011-11-392324.

Faget, J., Bendriss-Vermare, N., Gobert, M., Durand, I., Olive, D., Biota, C., Bachelot, T., Treilleux, I., Goddard-Leon, S., Lavergne, E., et al. (2012). ICOS-ligand expression on plasmacytoid dendritic cells supports breast cancer progression by promoting the accumulation of immunosuppressive CD4+ T cells. Cancer Res. *72*, 6130–6141. https://doi.org/10.1158/0008-5472.CAN-12-2409.

Feuerer, M., Rocha, M., Bai, L., Umansky, V., Solomayer, E.F., Bastert, G., Diel, I.J., and Schirrmacher, V. (2001). Enrichment of memory T cells and other profound immunological changes in the bone marrow from untreated breast cancer patients. Int. J. Cancer *92*, 96–105.

Feuerer, M., Beckhove, P., Garbi, N., Mahnke, Y., Limmer, A., Hommel, M., Hämmerling, G.J., Kyewski, B., Hamann, A., Umansky, V., and Schirrmacher, V. (2003). Bone marrow as a priming site for T-cell responses to blood-borne antigen. Nat. Med. *9*, 1151–1157. https://doi.org/10.1038/nm914.

Fujisaki, J., Wu, J., Carlson, A.L., Silberstein, L., Putheti, P., Larocca, R., Gao, W., Saito, T.I., Celso, C.L., Tsuyuzaki, H., et al. (2011). In vivo imaging of Treg cells providing immune privilege to the haematopoietic stem-cell niche. Nature *474*, 216–219. https://doi.org/10.1038/nature10160.

Gale, K.B., Ford, A.M., Repp, R., Borkhardt, A., Keller, C., Eden, O.B., and Greaves, M.F. (1997). Backtracking leukemia to birth: identification of clonotypic gene fusion sequences in neonatal blood spots. Proc. Natl. Acad. Sci. U S A *94*, 13950–13954. https://doi.org/10.1073/pnas.94.25.13950.

Geoerger, B., Kang, H.J., Yalon-Oren, M., Marshall, L.V., Vezina, C., Pappo, A., Laetsch, T.W., Petrilli, A.S., Ebinger, M., Toporski, J., et al. (2020). Pembrolizumab in paediatric patients with advanced melanoma or a PD-L1-positive, advanced, relapsed, or refractory solid tumour or lymphoma (KEYNOTE-051): interim analysis of an open-label, single-arm, phase 1–2 trial. Lancet Oncol. *21*, 121–133. https://doi.org/10.1016/S1470-2045(19)30671-0.

Greaves, M.F., and Wiemels, J. (2003). Origins of chromosome translocations in childhood leukaemia. Nat. Rev. Cancer *3*, 639–649. https://doi.org/10.1038/nrc1164.

Greaves, M.F., Maia, A.T., Wiemels, J.L., and Ford, A.M. (2003). Leukemia in twins: lessons in natural history. Blood *102*, 2321–2333. https://doi.org/10.1182/blood-2002-12-3817.

Han, Y., Dong, Y., Yang, Q., Xu, W., Jiang, S., Yu, Z., Yu, K., and Zhang, S. (2018). Acute myeloid leukemia cells express ICOS ligand to promote the expansion of regulatory T cells. Front. Immunol. *9*, 2227. https://doi.org/10.3389/fimmu.2018.02227.

Hanahan, D., and Weinberg, R.A. (2011). Hallmarks of cancer: the next generation. Cell *144*, 646–674. https://doi.org/10.1016/j.cell.2011.02.013.

Hirata, Y., Furuhashi, K., Ishii, H., Li, H.W., Pinho, S., Ding, L., Robson, S.C., Frenette, P.S., and Fujisaki, J. (2018). CD150high bone marrow Tregs maintain hematopoietic stem cell quiescence and immune privilege via adenosine. Cell Stem Cell *22*, 445–453.e5. https://doi.org/10.1016/j.stem.2018.01.017.

Hirata, Y., Kakiuchi, M., Robson, S.C., and Fujisaki, J. (2019). CD150high CD4 T cells and CD150high regulatory T cells regulate hematopoietic stem cell quiescence via CD73. Haematologica *104*, 1136–1142. https://doi.org/10.3324/haematol.2018.198283.

Hotfilder, M., Röttgers, S., Rosemann, A., Schrauder, A., Schrappe, M., Pieters, R., Jürgens, H., Harbott, J., and Vormoor, J. (2005). Leukemic stem cells in childhood high-risk ALL/t(9;22) and t(4;11) are present in primitive lymphoid-restricted CD34+CD19− cells) Are Present in Primitive Lymphoid-Restricted CD34+CD19− Cells. Cancer Res. *65*, 1442–1449. https://doi.org/10.1158/0008-5472.CAN-04-1356.

Hutloff, A., Dittrich, A.M., Beier, K.C., Eljaschewitsch, B., Kraft, R., Anagnostopoulos, I., and Kroczek, R.A. (1999). ICOS is an inducible T-cell co-stimulator structurally and functionally related to CD28. Nature *397*, 263–266. https://doi.org/10.1038/16717.

Ito, T., Hanabuchi, S., Wang, Y.H., Park, W.R., Arima, K., Bover, L., Qin, F.X.F., Gilliet, M., and Liu, Y.J. (2008). Two functional subsets of FOXP3+ regulatory T cells in human thymus and periphery. Immunity *28*, 870–880. https://doi.org/10.1016/j.immuni.2008.03.018.

Iwata, R., Hyoung Lee, J., Hayashi, M., Dianzani, U., Ofune, K., Maruyama, M., Oe, S., Ito, T., Hashiba, T., Yoshimura, K., et al. (2019). ICOSLG-mediated regulatory T cell expansion and IL-10 production promote progression of glioblastoma. Neuro Oncol. *22*, 333–344. noz204. https://doi.org/10.1093/neuonc/noz204.

Kang, H., Wilson, C.S., Harvey, R.C., Chen, I.M., Murphy, M.H., Atlas, S.R., Bedrick, E.J., Devidas, M., Carroll, A.J., Robinson, B.W., et al. (2012). Gene expression profiles predictive of outcome and age in infant acute lymphoblastic leukemia: a Children's Oncology Group study. Blood *119*, 1872–1881. https://doi.org/10.1182/blood-2011-10-382861.

Khayyamian, S., Hutloff, A., Büchner, K., Gräfe, M., Henn, V., Kroczek, R.A., and Mages, H.W. (2002). ICOS-ligand, expressed on human endothelial cells, costimulates Th1 and Th2 cytokine secretion by memory CD4+ T cells. Proc. Natl. Acad. Sci. U S A *99*, 6198–6203. https://doi.org/10.1073/pnas.092576699.

Kowarz, E., Löscher, D., and Marschalek, R. (2015). Optimized Sleeping Beauty transposons rapidly generate stable transgenic cell lines. Biotechnol. J. *10*, 647–653. https://doi.org/10.1002/biot.201400821.

Kühn, A., Löscher, D., and Marschalek, R. (2016). The IRX1/HOXA connection: insights into a novel t(4;11)- specific cancer mechanism. Oncotarget *7*, 35341–35352. https://doi.org/10.18632/oncotarget.9241.

Kumar, B., Garcia, M., Weng, L., Jung, X., Murakami, J.L., Hu, X., McDonald, T., Lin, A., Kumar, A.R., DiGiusto, D.L., et al. (2018). Acute myeloid leukemia transforms the bone marrow niche into a leukemia-permissive microenvironment through exosome secretion. Leukemia *32*, 575–587. https://doi.org/10.1038/leu.2017.259.

Lee, H.-J., Kim, S.N., Jeon, M.S., Yi, T., and Song, S.U. (2017). ICOSL expression in human bone marrow-derived mesenchymal stem cells promotes induction of regulatory T cells. Sci. Rep. *7*, 44486. https://doi.org/10.1038/srep44486.

le Viseur, C., Hotfilder, M., Bomken, S., Wilson, K., Röttgers, S., Schrauder, A., Rosemann, A., Irving, J., Stam, R.W., Shultz, L.D., et al. (2008). In childhood acute lymphoblastic leukemia, blasts at different stages of immunophenotypic maturation have stem cell properties. Cancer Cell *14*, 47–58. https://doi.org/10.1016/j.ccr.2008.05.015.

Li, D.-Y., and Xiong, X.-Z. (2020). ICOS+ Tregs: a functional subset of Tregs in immune diseases. Front. Immunol. *11*, 2104. https://doi.org/10.3389/fimmu.2020.02104.

Li, S., Miao, T., Sebastian, M., Bhullar, P., Ghaffari, E., Liu, M., Symonds, A., and Wang, P. (2012). The transcription factors Egr2 and Egr3 are essential for the control of inflammation and antigen-induced proliferation of B and T cells. Immunity *37*, 685–696. https://doi.org/10.1016/j.immuni.2012.08.001.

Li, R., Wang, Y., Cheng, H., Liu, G., Cheng, T., Liu, Y., and Liu, L. (2017). System modeling reveals the molecular mechanisms of HSC cell cycle alteration mediated by Maff and Egr3 under leukemia. BMC Syst. Biol. *11*, 91. https://doi.org/10.1186/s12918-017-0467-4.

Löhning, M., Hutloff, A., Kallinich, T., Mages, H.W., Bonhagen, K., Radbruch, A., Hamelmann, E., and Kroczek, R.A. (2003). Expression of ICOS in vivo defines CD4+ effector T cells with high inflammatory potential and a strong bias for secretion of interleukin 10. J. Exp. Med. *197*, 181–193. https://doi.org/10.1084/jem.20020632.

Mariette, X., Bombardieri, M., Alevizos, I., Moate, R., Sullivan, B., Noaiseh, G., Kvarnström, M., Rees, W., Wang, L., Illei, G., et al. (2019). A Phase 2a Study of MEDI5872 (AMG557), a Fully Human Anti-ICOS Ligand Monoclonal Antibody in Patients with Primary Sjögren's Syndrome. In ACR Meeting Abstracts. https://acrabstracts.org/abstract/a-phase-2a-study-of-medi5872-amg557-a-fully-human-anti-icos-ligand-monoclonal-antibody-in-patients-with-primary-sjogrens-syndrome/.

Martin-Orozco, N., Li, Y., Wang, Y., Liu, S., Hwu, P., Liu, Y.J., Dong, C., and Radvanyi, L. (2010). Melanoma cells express ICOS ligand to promote the activation and expansion of T-regulatory cells. Cancer Res. *70*, 9581–9590. https://doi.org/10.1158/0008-5472.CAN-10-1379.

Medyouf, H. (2017). The microenvironment in human myeloid malignancies: emerging concepts and therapeutic implications. Blood *129*, 1617–1626. https://doi.org/10.1182/blood-2016-11-696070.

Metsalu, T., and Vilo, J. (2015). ClustVis: a web tool for visualizing clustering of multivariate data using Principal Component Analysis and heatmap. Nucleic Acids Res. *43*, W566–W570. https://doi.org/10.1093/nar/gkv468.

Meyer, C., BurmeisTer, T., Gröger, D., Tsaur, G., Fechina, L., Renneville, A., Sutton, R., Venn, N.C., EMerenciano, M., Pombo-de-Oliveira, M.S., et al. (2018). The MLL recombinome of acute leukemias in 2017. Leukemia *32*, 273–284. https://doi.org/10.1038/leu.2017.213.

Min, I.M., Pietramaggiori, G., Kim, F.S., Passegué, E., Stevenson, K.E., and Wagers, A.J. (2008). The transcription factor EGR1 controls both the proliferation and localization of hematopoietic stem cells. Cell Stem Cell *2*, 380–391. https://doi.org/10.1016/j.stem.2008.01.015.

Morrison, S.J., and Scadden, D.T. (2014). The bone marrow niche for haematopoietic stem cells. Nature *505*, 327–334. https://doi.org/10.1038/nature12984.

Moudgil, A., Wilkinson, M.N., Chen, X., He, J., Cammack, A.J., Vasek, M.J., Lagunas, T., Jr., Qi, Z., Lalli, M.A., Guo, C., et al. (2020). Self-reporting transposons enable simultaneous readout of gene expression and transcription factor binding in single cells. Cell *182*, 992–1008.e21. https://doi.org/10.1016/j.cell.2020.06.037.

Osmond, D.G. (1994). Production and selection of B lymphocytes in bone marrow: lymphostromal interactions and apoptosis in normal, mutant and transgenic mice. Adv. Exp. Med. Biol. *355*, 15–20. https://doi.org/10.1007/978-1-4615-2492-2_3.

Parkinson, R.M., Collins, S.L., Horton, M.R., and Powell, J.D. (2014). Egr3 induces a Th17 response by promoting the development of γδ T cells. PLoS One *9*, e87265. https://doi.org/10.1371/journal.pone.0087265.

Petroff, M.G., Kharatyan, E., Torry, D.S., and Holets, L. (2005). The immunomodulatory proteins B7-DC, B7-H2, and B7-H3 are differentially expressed across gestation in the human placenta. Am. J. Pathol. *167*, 465–473. https://doi.org/10.1016/S0002-9440(10)62990-2.

Pieters, R., Schrappe, M., De Lorenzo, P., Hann, I., De Rossi, G., Felice, M., Hovi, L., LeBlanc, T., Szczepanski, T., Ferster, A., et al. (2007). A treatment protocol for infants younger than 1 year with acute lymphoblastic leukaemia (Interfant-99): an observational study and a multicentre randomised trial. Lancet (Lond, Engl) *370*, 240–250. https://doi.org/10.1016/S0140-6736(07)61126-X.

Pieters, R., De Lorenzo, P., Ancliffe, P., Aversa, L.A., Brethon, B., Biondi, A., Campbell, M., Escherich, G., Ferster, A., Gardner, R.A., et al. (2019). Outcome of infants younger than 1 Year with acute lymphoblastic leukemia treated with the interfant-06 protocol: results from an international phase III randomized study. J. Clin. Oncol. *37*, 2246–2256. https://doi.org/10.1200/JCO.19.00261.

Pontarini, E., Verstappen, G.M., Grigoriadou, S., Kroese, F.G.M., Bootsma, H., and Bombardieri, M. (2020). Blocking T cell co-stimulation in primary Sjögren's syndrome: rationale, clinical efficacy and modulation of peripheral and salivary gland biomarkers. Clin. Exp. Rheumatol. *38*, 222–227.

Rice, S., Jackson, T., Crump, N.T., Fordham, N., Elliott, N., O'Byrne, S., Fanego, M.M.L., Addy, D., Crabb, T., Dryden, C., et al. (2021). A human fetal liver-derived infant MLL-AF4 acute lymphoblastic leukemia model reveals a distinct fetal gene expression program. Nat. Commun. *12*, 6905. https://doi.org/10.1038/s41467-021-27270-z.

Riella, L.V., Dada, S., Chabtini, L., Smith, B., Huang, L., Dakle, P., Mfarrej, B., D'Addio, F., Adams, L.T., Kochupurakkal, N., et al. (2013). B7h (ICOS-L) maintains tolerance at the fetomaternal interface. Am. J. Pathol. *182*, 2204–2213. https://doi.org/10.1016/j.ajpath.2013.02.014.

Safford, M., Collins, S., Lutz, M.A., Allen, A., Huang, C.T., Kowalski, J., Blackford, A., Horton, M.R., Drake, C., Schwartz, R.H., and Powell, J.D. (2005). Egr-2 and Egr-3 are negative regulators of T cell activation. Nat. Immunol. *6*, 472–480. https://doi.org/10.1038/ni1193.

Salvany-Celades, M., van der Zwan, A., Benner, M., Setrajcic-Dragos, V., Bougleux Gomes, H.A., Iyer, V., Norwitz, E.R., Strominger, J.L., and Tilburgs, T. (2019). Three types of functional regulatory T cells control T cell responses at the human maternal-fetal interface. Cell Rep. *27*, 2537–2547.e5. https://doi.org/10.1016/j.celrep.2019.04.109.

Sandelin, A., Alkema, W., Engström, P., Wasserman, W.W., and Lenhard, B. (2004). JASPAR: an open-access database for eukaryotic transcription factor binding profiles. Nucleic Acids Res. *32*, D91–D94. https://doi.org/10.1093/nar/gkh012.

Stam, R.W., Schneider, P., Hagelstein, J.A.P., van der Linden, M.H., Stumpel, D.J.P.M., de Menezes, R.X., de Lorenzo, P., Valsecchi, M.G., and Pieters, R. (2010). Gene expression profiling–based dissection of MLL translocated and MLL germline acute lymphoblastic leukemia in infants. Blood *115*, 2835–2844. https://doi.org/10.1182/blood-2009-07-233049.

Sullivan, B.A., Tsuji, W., Kivitz, A., Peng, J., Arnold, G.E., Boedigheimer, M.J., Chiu, K., Green, C.L., KAliyAperumAl, A., Wang, C., et al. (2016). Inducible T-cell co-stimulator ligand (ICOSL) blockade leads to selective inhibition of anti-KLH IgG responses in subjects with systemic lupus erythematosus. Lupus Sci. Med. *3*, e000146. https://doi.org/10.1136/lupus-2016-000146.

Svensson-Arvelund, J., Mehta, R.B., Lindau, R., Mirrasekhian, E., Rodriguez-Martinez, H., Berg, G., Lash, G.E., Jenmalm, M.C., and Ernerudh, J. (2015). The human fetal placenta promotes tolerance against the semiallogeneic fetus by inducing regulatory T cells and homeostatic M2 macrophages. J. Immunol. *194*, 1534–1544. https://doi.org/10.4049/jimmunol.1401536.

Swallow, M.M., Wallin, J.J., and Sha, W.C. (1999). B7h, a novel costimulatory homolog of B7.1 and B7.2, is induced by TNFα. Immunity *11*, 423–432. https://doi.org/10.1016/S1074-7613(00)80117-X.

Symeonidou, V., and Ottersbach, K. (2021). HOXA9/IRX1 expression pattern defines two subgroups of infant MLL-AF4-driven acute lymphoblastic leukemia. Exp. Hematol. *93*, 38–43.e5. https://doi.org/10.1016/j.exphem.2020.10.002.

Takahata, Y., Nomura, A., Takada, H., Ohga, S., Furuno, K., Hikino, S., Nakayama, H., Sakaguchi, S., and Hara, T. (2004). CD25+CD4+ T cells in human cord blood: an immunoregulatory subset with naive phenotype and specific expression of forkhead box p3 (Foxp3) gene. Exp. Hematol. *32*, 622–629. https://doi.org/10.1016/j.exphem.2004.03.012.

Tallen, G., Ratei, R., Mann, G., Kaspers, G., Niggli, F., Karachunsky, A., Ebell, W., Escherich, G., Schrappe, M., Klingebiel, T., et al. (2010). Long-term outcome in children with relapsed acute lymphoblastic leukemia after time-point and site-of-relapse stratification and intensified short-course multidrug chemotherapy: results of trial

ALL-REZ BFM 90. J. Clin. Oncol. 2339–2347. https://doi.org/10.1200/JCO.2009.25.1983.

Tang, C., Li, M.H., Chen, Y.L., Sun, H.Y., Liu, S.L., Zheng, W.W., Zhang, M.Y., Li, H., Fu, W., Zhang, W.J., et al. (2018). Chemotherapy-induced niche perturbs hematopoietic reconstitution in B-cell acute lymphoblastic leukemia. J. Exp. Clin. Cancer Res. *37*, 204. https://doi.org/10.1186/s13046-018-0859-3.

Tilburgs, T., Roelen, D.L., van der Mast, B.J., de Groot-Swings, G.M., Kleijburg, C., Scherjon, S.A., and Claas, F.H. (2008). Evidence for a selective migration of fetus-specific CD4+CD25bright regulatory T cells from the peripheral blood to the decidua in human pregnancy. J. Immunol. *180*, 5737–5745. https://doi.org/10.4049/jimmunol.180.8.5737.

Trentin, L., Giordan, M., Dingermann, T., Basso, G., te Kronnie, G., and Marschalek, R. (2009). Two independent gene signatures in pediatric t(4;11) acute lymphoblastic leukemia patients. Eur. J. Haematol. *83*, 406–419. https://doi.org/10.1111/j.1600-0609.2009.01305.x.

Vocanson, M., Rozieres, A., Hennino, A., Poyet, G., Gaillard, V., Renaudineau, S., Achachi, A., Benetiere, J., Kaiserlian, D., Dubois, B., and Nicolas, J.F. (2010). Inducible costimulator (ICOS) is a marker for highly suppressive antigen-specific T cells sharing features of TH17/TH1 and regulatory T cells. J. Allergy Clin. Immunol. *126*, 280–289.e7. https://doi.org/10.1016/j.jaci.2010.05.022.

Wiemels, J.L., CazzaniGa, G., Daniotti, M., Eden, O., Addison, G., Masera, G., Saha, V., Biondi, A., and Greaves, M. (1999). Prenatal origin of acute lymphoblastic leukaemia in children. Lancet *354*, 1499–1503. https://doi.org/10.1016/s0140-6736(99)09403-9.

Yang, W., Lee, K.W., Srivastava, R.M., Kuo, F., Krishna, C., Chowell, D., Makarov, V., Hoen, D., Dalin, M.G., Wexler, L., et al. (2019). Immunogenic neoantigens derived from gene fusions stimulate T cell responses. Nat. Med. *25*, 767–775. https://doi.org/10.1038/s41591-019-0434-2.

Zamora, A.E., Crawford, J.C., Allen, E.K., Guo, X.J., Bakke, J., Carter, R.A., Abdelsamed, H.A., Moustaki, A., Li, Y., Chang, T.C., et al. (2019). Pediatric patients with acute lymphoblastic leukemia generate abundant and functional neoantigen-specific CD8 $^{+}$ T cell responses. Sci. Transl. Med. *11*, eaat8549. https://doi.org/10.1126/scitranslmed.aat8549.

Zhang, Y., Luo, Y., Qin, S.L., Mu, Y.F., Qi, Y., Yu, M.H., and Zhong, M. (2016). The clinical impact of ICOS signal in colorectal cancer patients. Oncoimmunology *5*, e1141857. https://doi.org/10.1080/2162402X.2016.1141857.

Zou, L., Barnett, B., Safah, H., LaRussa, V.F., Evdemon-Hogan, M., Mottram, P., Wei, S., David, O., Curiel, T.J., and Zou, W. (2004). Bone marrow is a reservoir for CD4+CD25+ regulatory T cells that Traffic through CXCL12/CXCR4 signals. Cancer Res. *64*, 8451–8455. https://doi.org/10.1158/0008-5472.CAN-04-1987.

STAR★METHODS

KEY RESOURCES TABLE

REAGENT or RESOURCE	SOURCE	IDENTIFIER
Antibodies		
Goat Anti-Rabbit IgG, polyclonal antibody, Horseradish Peroxidase conjugated (1:10000; WB)	abcam	Abcam Cat# ab6721, RRID: AB_955447
DYKDDDDK Tag (D6W5B) Rabbit, monoclonal antibody, unconjugated (1/1,000 WB and ChIP)	Cell Signaling Technology	Cell Signaling Technology Cat# 14793, RRID: AB_2572291
Rabbit Anti-Actin, polyclonal antibody, unconjugated (1/1,000 WB)	Sigma-Aldrich	Sigma-Aldrich Cat# A2066, RRID: AB_476693
Rabbit Recombinant Anti-ICOS Ligand/ICOSL, monoclonal antibody, unconjugated (1/1,000 WB)	abcam	ab209262 RRID not found
Mouse Anti-Human CD3, monoclonal antibody, APC-H7 conjugated (flow cytometry)	BD	BD Biosciences Cat# 560176, RRID: AB_1645475
Mouse Anti-Human CD4, monoclonal antibody, PE-Cy7 conjugated (flow cytometry)	BD	BD Biosciences Cat# 557852, RRID: AB_396897
Mouse Anti-Human CD8, monoclonal antibody, BV510 conjugated (flow cytometry)	BD	BD Biosciences Cat# 563919, RRID: AB_2722546
Mouse Anti-Human CD25 (IL-2 Receptor α), monoclonal antibody, BV421 conjugated (flow cytometry)	BD	BD Biosciences Cat# 564033, RRID: AB_2738555
Mouse Anti-Human FoxP3, monoclonal antibody, AF647 conjugated (flow cytometry)	BD	BD Biosciences Cat# 561184, RRID: AB_10584328
Mouse Anti-Human CD278 (ICOS), monoclonal antibody, BB515 conjugated (flow cytometry)	BD	BD Biosciences Cat# 564549, RRID: AB_2738840
Mouse Anti-Human B7-h2, monoclonal antibody, neutralizing, unconjugated (neutralization assays)	RnD Systems	R and D Systems Cat# MAB165, RRID: AB_2122734
Mouse IgG1 kappa isotype control, functional grade (neutralization assays)	Thermo Fisher	Thermo Fisher Scientific Cat# 16-4714-85, RRID: AB_470162
Bacterial and virus strains		
NEB® 5-alpha competent *E. coli*; DH5α™ derivative	NEB	NEB Cat# C2987
Biological samples		
see Tables		
Chemicals, peptides, and recombinant proteins		
Q5® High-Fidelity DNA Polymerase	NEB	NEB Cat# M0491L
SuperScript™ II Reverse Transcriptase	Invitrogen	Invitrogen 18064071
Annexin V Pacific Blue	Invitrogen	Invitrogen A35122
SfiI restriction enzyme	NEB	NEB Cat# R0123L
T4 DNA ligase	NEB	NEB Cat# M0202S
Clarity Max Western ECL Substrate	Bio-Rad	Bio-Rad Cat# 1705062
Protease inhibitory cocktail tablets	Roche	Roche 4693116001
Critical commercial assays		
Amaxa™ Cell Line Nucleofector™ Kit R	Lonza	VCA-1001
Pierce™ BCA Protein Assay Kit (23225, thermo scientific)	Thermo Scientific	Thermo Scientific 23225
IL-10 (human) ELISA Kit	Enzo	Enzo ADI-900-036
IL-2 ELISA Kit (human)	Aviva	Aviva OKBB00179

(*Continued on next page*)

Continued

REAGENT or RESOURCE	SOURCE	IDENTIFIER
Accel-NGS® 2S plus DNA library kit	Swift Biosciences	Swift Biosciences 21024
Swift Unique Dual Indexing Primer Kit	Swift Biosciences	Swift Biosciences X9096
Accel-NGS 2S Truncated Adapters	Swift Biosciences	Swift Biosciences 28196
Deposited data		
All Chip-Seq data have been deposited in the NCBI Geobus database		GSE205652
Experimental models: Cell lines		
SEM	DSMZ	ACC 546
Oligonucleotides		
GAPDH_fwd_short 5′-GGTCACCAGGGCTGC-3′	this paper	N/A
GAPDH_rev_short 5′-CGTTCTCAGCCTTGA-3′	this paper	N/A
ICOSLG_fwd 5′-TGACATCGGAGAGAGAGACAAG-3′	this paper	N/A
ICOSLG_rev 5′-ACGCTTTTGAAAGGGCCTCA-3′	this paper	N/A
EGR3.SfiI_fwd 5′-GGCCTCTGAGGCCACCATGAC CGGCAAACTCGCC-3′	this paper	N/A
EGR3cFLAG.SfiI_rev 5′-GGCCTGACAGGCCTTACTTATCG TCATCGTCCTTGTAGTC-3′	this paper	N/A
EGR3.SF1_fwd 5′-GGCCTAGCAAGACACCGC-3′	this paper	N/A
HOXA9_fwd_short 5′-CCACGCTTGACACTCACACT-3′	this paper	N/A
HOXA9_rev_short 5′-AGTTGGCTGCTGGGTTATTG-3′	this paper	N/A
IRX1_fwd_short 5′-GGATCTCAGCCTCTTCTCG-3′	this paper	N/A
IRX1_rev_short 5′-GTGGAGACCTGCGTGAGG-3′	this paper	N/A
EGR3_fwd_short 5′-CAGCGACTCGGTAGTCCATT-3′	this paper	N/A
EGR3_rev_short 5′-TAGGTCACGGTCTTGTTGCC-3′	this paper	N/A
ICOSLG_fwd_short 5′-AGTCCGGAGACAGAGCTCAC-3′	this paper	N/A
ICOSLG_rev_short 5′-CAGTCTGGGAGTCCATGCTC-3′	this paper	N/A
ICOSLG_fwd_ChIP1 5′-ACCGGGACCCATGGCA-3′	this paper	N/A
ICOSLG_rev_ChIP1 5′-CTCCCTCCTTCCAGCGTTC-3′	this paper	N/A
ICOSLG_fwd_ChIP2 5′-GTGAGCCGGGGAAGGA-3′	this paper	N/A
ICOSLG_rev_ChIP2 5′-ATGGGTCCCGGTGCCA-3′	this paper	N/A
ICOSLG_fwd_ChIP3 5′-GCAGAGCCGAACTTTCCG-3′	this paper	N/A
ICOSLG_rev_ChIP3 5′-TGGAGGCAGCCGTGTC-3′	this paper	N/A
ICOSLG_fwd_ChIP4 5′-CCTCAGAGCCAGTGTTAAGC-3′	this paper	N/A
ICOSLG_rev_ChIP4 5′-CGCATGCATGAATGGAAGGA-3′	this paper	N/A
ICOSLG_fwd_ChIP5 5′-GCCCTGCCCAGCTCTT-3′	this paper	N/A
ICOSLG_rev_ChIP5 5′-CAGGCCACGCTGAGAGAC-3′	this paper	N/A
ICOSLG_fwd_ChIP6 5′-GCTCTCCAAGGCCAGCTG-3′	this paper	N/A
ICOSLG_rev_ChIP6 5′-AAGCTGTCACTCCTGGTTCA-3′	this paper	N/A
Recombinant DNA		
pSBtet_Puro sleeping beauty vector backbone	Kowarz et al. (2015)	AddGene #60507
EGR3 open reading frame	this paper	HEK293T cDNA
Sleeping beauty transposase plasmid pcGLobin-SB100$_{XCO}$	Moudgil et al. (2020)	AddGene #154887
Software and algorithms		
GraphPad Prism 7.01	GraphPad Software Inc.	GraphPad Prism 7.01
ClustVis (Metsalu and Vilo, 2015)	open source	N/A

(*Continued on next page*)

Continued		
REAGENT or RESOURCE	SOURCE	IDENTIFIER
TrimGalore	open source	N/A
Bowtie2	open source	N/A
SAMtools	open source	N/A
MACS3	open source	N/A
R package "ChIPseeker"	open source	N/A
R package "encodeChIPqc"	open source	N/A
python tool "deepTools"	open source	N/A
Integrative Genomics Viewer (IGV)	open source	N/A
Other		
Low Fluorescence PVDF Western Membrane	Abcam	Abcam Cat# ab133411
Precision Plus Protein™ All Blue Standards; marker used for Western Blots with fluorescence detection	Bio-Rad	Bio-Rad Cat# 1610373EDU
Color Protein Standard Broad Range	NEB	NEB P7719S

RESOURCE AVAILABILITY

Lead contact

Further information and requests for resources and reagents should be directed to and will be fulfilled by the Lead Contact, Rolf Marschalek (Rolf.marschalek@em.uni-frankfurt.de).

Materials availability

All unique/stable reagents generated in this study are available from the Lead Contact with a completed Materials Transfer Agreement.

Data and code availability

All experimental data or any additional information required to reanalyze the data reported in this paper are available from the Lead contact. This paper does not report original code. Any additional information required to reanalyze the data reported in this paper is available from the Lead contact upon request.

EXPERIMENTAL MODEL AND SUBJECT DETAILS

Animals

Not applicable.

Cell culture

SEM cells (ACC 546) and isolated primary T-cells were cultivated under sterile conditions. SEM cells were maintained in RPMI 1640 (RPMI-HA, Capricorn Scientific) supplemented with 10% FBS (FBS-11A, Capricorn Scientific), 2 mM L-glutamine (STA-B, Capricorn Scientific), 100 U/ml penicillin and 100 µg/mL streptomycin (PS-B, Capricorn Scientific), preheated to 37°C prior to use. Primary T-cells were maintained in DMEM high glucose (DMEM-HPA, Capricorn Scientific) supplemented with 10% human plasma (derived from each donor), 2 mM L-glutamine (STA-B, Capricorn Scientific), 100 U/ml penicillin and 100 µg/ml streptomycin (PS-B, Capricorn Scientific), preheated to 37°C prior to use. Cells were kept at 37°C in 5% CO_2 and a relative humidity of 95%. SEM cells were passaged twice a week with complete media exchange maintaining a density of ~1 x 10^6 cells/mL. For this, cell suspension was centrifuged at 200 x g for 5 min and subsequently cell pellet was resuspended in new prewarmed media. T-cells were immediately activated following isolation as described below and underwent co-culture experiments, thus no passaging was necessary.

Co-culture study

1x10^6 SEM::EGR3 or SEM::mock were co-cultured for 48h with 5x10^5 $CD4^+$ T-cells and 5x10^5 $CD8^+$ T-cells in 1 mL of DMEM-HPA (Capricorn Scientific) supplemented with 10% human plasma (derived from each donor), 2 mM L-glutamine (STA-B, Capricorn Scientific), 100 U/ml penicillin and 100 µg/mL streptomycin (PS-B, Capricorn Scientific), preheated to 37°C prior to use. T-lymphocytes were isolated from the

peripheral blood mononuclear cells (PBMC) of healthy donors using magnetic bead separation as described below. Prior to co-culture, isolated T-cells were stimulated with the T-cell Acitvation/Expansion Kit human (130-091-441, Mitlenyi Biotec) for 24h according to the manufacturer's recommendations. SEM::EGR3 and SEM::mock were induced with 1 μg/mL Doxycycline 24h prior to co-culture and 20 μg/mL neutralizing monoclonal mouse α-human ICOSLG antibody (RnD Systems®) or mouse IgG1 isotype control (Invitrogen™) were added 2h prior to co-culture. After 48h of co-culture cells were collected and stained with FACS antibodies and supernatant immediately frozen in liquid nitrogen and stored for ELISA experiments.

METHOD DETAILS

Plasmid cloning

EGR3 open reading frame (ORF) was amplified from HEK293T cDNA with the primers EGR3.SfiI_fwd and EGR3cFLAG.SfiI_rev using Q5® High-Fidelity DNA Polymerase (NEB, M0491L). EGR3.SfiI_fwd adds the 5'-SfiI restriction site GGCCTCTGAGGCC upstream of ATG and EGR3cFLAG.SfiI_rev adds a FLAG (DYKDDDDK) tag to the ORF and the 3'-SfiI restriction site GGCCTGTCAGGCC downstream of TAA. Equipped with the SfiI restriction sites, the ORF was ligated into SfiI-digested pSBtet_Puro backbone (R0123L, NEB) using T4 DNA ligase (M0202S, NEB). The yielded plasmid pSBtet_EGR3cFLAG_Puro was sequence validated.

Establishment of the stable cell lines SEM::mock and SEM::EGR3

Electroporation of SEM cells was performed using the Nucleofector™ 2b device (AAB-1001, Lonza) together with the Amaxa™ Cell Line Nucleofector™ Kit R (VCA-1001) and the nucleofection program T-016 according to the manufacturer's recommendations. 0.1 μg sleeping beauty transposase plasmid pcGLobin-SB100$_{XCO}$ together with 1.9 μg sleeping beauty plasmid (pSBtet_ohneLuc_Puro = SEM::mock; pSBtet_EGR3cFLAG_Puro = SEM::EGR3; pSBtet_Luc_GP = green fluorescence postive control) were electroporated. pSBtet_ohneLuc_Puro and pSBtet_EGR3cFLAG_Puro do not have a fluorescence marker in their backbone to avoid interference in multicolor flow cytometry. To monitor transfection and selection efficiency with a fluorescence microscope, pSBtet_Luc_GP containing a GFP marker in the backbone was treated equally and served as a reporter. Cells were selected six times (once to twice per week) with Puromycin 2 μg/mL for 24-48h until all reporter cells displayed green fluorescence. Proof of transgene expression was performed using PCR and subsequent gel electroporation, qRT-PCR, and western blot 48h after induction of transgene expression with Doxycycline 1 μg/mL.

Human T-cell isolation

PBMC were isolated from the blood of healthy adult donors using Ficoll-Paque density gradient centrifugation. Therefore, 15 mL blood were diluted with 20 mL PBS (PBS-1A, Capricorn Scientific) supplemented with 0.5% BSA and overlayed with Lymphocyte Separation Media (MS00ZZ1002, Biowest) followed by 30 min centrifugation at 400 g without break leading to separation of plasma and PBMC from remaining blood cells. Plasma was stored for T-cell culture media preparation. PBMC layer was moved to another tube and resuspended in 50 mL PBS supplemented with 0.5% BSA followed by centrifugation at 400 g for 5 min with break. Pellet was resuspended in 10 mL RBC lysis buffer for human liquid (J62990, Alfa Aesar) and 10 min incubated at room temperature to lyse remaining erythrocytes. Afterwards, cell suspension was washed with 30 mL PBS supplemented with 0.5% BSA and isolated PBMC were counted. $CD4^+$ and $CD8^+$ cells were magnetically separated using CD4 Micro-Beads, human (130-045-101, Miltenyi Biotec) or CD8 MicroBeads, human (130-045-201, Miltenyi Biotec), MS columns (130-042-201, Miltenyi Biotec) and OctoMACS™ separator (130-042-109, Miltenyi Biotec) according to the manufacturer's protocols. Success of T-cell isolation was checked with flow cytometry prior to activation.

Gene expression analysis using qRT-PCR

RNA was extracted from ~5x10^7 SEM::mock and SEM::EGR3 48h after transgene induction with 1 μg/mL Doxycycline. cDNA was synthesized out of 2 μg RNA using random hexamer N6 primers and SuperScript™ II Reverse Transcriptase (18064071, Invitrogen). PCR primers used in the study are summarized in STAR Methods. qRT-PCR was performed with the StepOnePlus system. ΔC_T mean values were calculated out of triplicates using GAPDH expression as a reference, $\Delta\Delta C_T$ values are related to the respective expression of SEM::mock.

Protein expression analysis using Western blot experiments

Protein was extracted from ~5x10^7 SEM::mock and SEM::EGR3 48h after transgene induction with 1 μg/mL Doxycycline. Cells were lysed in 1 mL protein extraction buffer (150 mM NaCl, 10 mM Tris-HCl, 1mM EDTA, 1mM EGTA, 0.2 mM sodium ortho-vanadate, 0.2 mM PMSF, 1% Triton-X-100, 0.5% NP-40, freshly added protease inhibitory cocktail (4693116001, Roche) under constant agitation for 30 min at 4°C. Centrifugation at 400 g, 4°C enabled separation of the supernatant (= protein lysate) from cell debris. Protein lysate was quantified using Pierce™ BCA Protein Assay Kit (23225, Thermo Scientific) according to the manufacturer's recommendations. 20 μg protein lysate were electrophoretically separated using Mini-PROTEAN TGX Stain-Free Gels 4-15% (4568085, Bio-Rad) and Color Protein Standard Broad Range (P7719S, NEB). Proteins were blotted onto Low Fluorescence Western Memranes PVDF (ab133411, Abcam) in Towbin buffer (25 mM Tris, 192 mM Glycin, 15% methanol, 0.01% SDS, pH = 8.3) at 110 V for 70 min. Membranes were blocked using 5% BSA in TBS-T for 1h at room temperature and primary antibody incubation (1/1,000) performed o/n at 4°C. Membranes were washed with TBS-T and incubated with HRP-conjugated secondary antibody (1/10,000) for 1h at room temperature. Chemiluminescence detection was performed using Clarity™ Western ECL Substrate (170-5061, Bio-Rad) and ChemiDoc™ XRS+ system (1708265, Bio-Rad). Antibodies used for western blot are listed in STAR Methods.

Flow cytometry experiments

Cells were blocked and stained with FACS antibodies (BD Biosciences) according to the manufacturer's recommendations. Half of the cell suspension was stained with α-CD3, -CD4, -CD8, Annexin V and 7-AAD to assess the viability of the T-cells after co-culture. The remaining cells were stained with α-CD3, -CD4, -CD8, -CD25, -ICOS, fixed, permeabilized and stained with α-FOXP3. Cells were analysed with a BD FACSVerse™. The gating strategy is explained in Figure 6A. All antibodies used for this strategy are described in STAR Methods.

ELISA experiments

The IL-2 and IL-10 concentrations of the co-culture supernatants were assessed using IL-10 (human) ELISA Kit (ADI-900-036, Enzo) and IL-2 ELISA Kit (human) (OKBB00179, Aviva) according to the manufacturer's recommendations.

Chromatin immunoprecipitation qRT-PCR and sequencing

2x10^7 SEM::EGR3 and SEM::mock were induced with 1 μg/mL Doxycycline for 48h followed by ChIP procedure as described by Kühn et al., (2016). The transcription factor binding site prediction tool JASPAR (Sandelin et al., 2004) was used to detect potential EGR3 binding sites 1 kb up- and downstream of the transcription start site of *ICOSLG*. Six primer pairs were used to cover the nine highest scoring potential binding sites in qRT-PCR. Primers used for ChIP-qRT-PCR are summarized in STAR Methods. Antibodies used for ChIP are described in STAR Methods. The ChIP-Seq library was prepared using the Accel-NGS® 2S plus DNA library kit (21024, Swift Biosciences) together with Swift Unique Dual Indexing Primer Kit (X9096, Swift Biosciences) and Accel-NGS 2S Truncated Adapters (28196, Swift Biosciences) according to the manufacturer's recommendations with indexing by PCR (10 cycles). NGS was performed using the MiSeq system (SY-410-1003, Illumina) and the MiSeq Reagent Kit v2 (MS-102-2003, Illumina). The ChIP-Seq analysis was performed in several steps. As a first step, in order to remove adapters contamination, raw Illumina paired-end reads were processed with TrimGalore. In a second step, we mapped paired-end sequence reads against the human reference genome GRCh38 with Bowtie2. SAMtools was then used to convert the resulting sam files to bam files and to generate the index files. Once the chromatin immunoprecipitate (IP) and control (input) libraries have been aligned, we proceeded with the peak calling in order to determine the regions in which the IP signal is significantly higher than the input signal (=background). We performed the peak calling with the tool MACS3 with the option BAMPE active because of paired end reads. The result of the peak calling (narrowPeak file) was then used with the R package "ChIPseeker" to annotate the peaks to neighboring genes and genomics regions. We then performed a number of routine quality controls such as PCR bottleneck coefficient (PBC), fraction of reads in peaks (FriP) using the R package "encodeChIPqc" and fingerprint plot using "plotFingerprint" from the python tool "deepTools". In the final step we used the functions "bamCoverage" and "bamCompare" from "deepTools" to generate signal files in the bigwig format. We generated either separate bigwig files for IP and control with "bamCoverage" or a single bigwig file in which we subtracted the background noise from the IP with "bamCompare". Finally, the signal files, along with narrowPeak files and bam files, can be visualized using the Integrative Genomics

Viewer (IGV). Data have been deposited in the NCBI Geobus database with the accession number GSE205652.

Patient gene expression study

Informed consent was obtained for all patients by the respective study centers that provided patient RNA. All patients displayed a pro-B phenotype and were diagnosed between 0 and 12 months of age (infants). RNA was extracted from blood at day of initial diagnosis (dx cohort, n = 50) or relapse diagnosis (rel cohort, n = 18) by the respective study centers. The dx cohort is solely composed of t(4;11) iALL cases, the rel cohort is composed of different translocations as indicated in Table 2 . cDNA was synthesized out of 1 μg RNA as described above. *HOXA9*, *IRX1*, *EGR3* and *ICOSLG* gene expression was measured as triplicates using qRT-PCR (StepOnePlus system) and ΔC_T mean values were calculated using *GAPDH* expression as a reference. Relative expressions were calculated as ratio (reference/target) = $2^{CT(GAPDH) - CT(target)} = 2^{-\Delta CT}$. Pearson correlation was calculated for the gene expression datasets *IRX1*- > *EGR3*, *IRX1*- > *ICOSLG* and *EGR3*- > *ICOSLG* using GraphPad Prism software. Clinical outcome of the patients was provided by the study centers.

QUANTIFICATION AND STATISTICAL ANALYSIS

Statistical tests were performed using GraphPad Prism 7.01 and settings are indicated in figure legends. Principal component analysis (PCA) was performed using ClustVis (Metsalu and Vilo, 2015) with patient sample ΔC_T mean value assigned to the dx *ICOSLG*^{hi}, dx *ICOSLG*^{lo} or rel cohort, respectively. PCA was performed as singular value decomposition (SVD) and unit variance scaling for rows was applied. The PCA heatmap was generated with *correlation* as clustering distance for rows, *average* as clustering method for rows and columns, and *Manhattan* as clustering distance for columns.

Kaplan-Meier plotting and log rank test were performed using GraphPad Prism 7.01. EFS was defined as the time from diagnosis to first failure (induction failure, relapse, death, or second malignant neoplasm). Time was censored at last follow-up if no events had been observed. Curves were estimated with Kaplan-Meier, with SEs calculated according to Greenwood, and compared using the log rank test.